INFLUENCE OF TURBULENCE PROMOTER GEOMETRY ON FLOW PATTERN IN CROSS-FLOW MEMBRANE ULTRAFILTRATION

SUPAWADEE WANTHAMANEE

A THESIS SUBMITTED IN PARTIAL FULFILLMENT
OF THE REQUIREMENTS FOR THE DEGREE OF
MASTER OF ENGINEERING IN CHEMICAL ENGINEERING
FACULTY OF ENGINEERING
KING MONGKUT'S INSTITUTE OF TECHNOLOGY LADKRABANG
2013

หัวข้อวิทยานิพนธ์ อิทธิพลของรูปร่างตัวสนับสนุนความปั่นป่วนต่อรูปแบบการไหลในเมมเบรนอัลตราฟิลเตรชันชนิดไหลขวาง

นักศึกษา นางสาวสุภาวดี วรรธะมานี

รหัสประจำตัว 52611420

ปริญญา วิศวกรรมศาสตรมหาบัณฑิต

สาขาวิชา วิศวกรรมเคมี

พ.ศ. 2556

อาจารย์ที่ปรึกษาวิทยานิพนธ์ ดร.สันติ วัฒนานุสรณ์

บทคัดย่อ

งานวิจัยนี้ศึกษาอิทธิพลของรูปร่างตัวสนับสนุนความปั่นป่วน (turbulence promoter) ต่อรูปแบบการไหลในเมมเบรนอัลตราฟิลเตรชันชนิดไหลขวางด้วยพลศาสตร์ของไหลเชิงคำนวณ (Computational Fluid Dynamics; CFD) โดยแบบจำลองถูกคำนวณด้วยโปรแกรม FLUENT ซึ่งใช้วิธีปริมาตรสืบเนื่อง ผลการจำลองถูกนำมาเปรียบเทียบกับผลการทดลองเพื่อยืนยันความถูกต้องของแบบจำลองที่สร้างขึ้น ตัวสนับสนุนความปั่นป่วนที่ทำการศึกษามี 6 รูปแบบคือ แบบทรงกระบอก สี่เหลี่ยมจัตุรัส เพชร ปรีซึมแบบที่ 1 ปรีซึมแบบที่ 2 และแผ่นสี่เหลี่ยมบาง ผลการจำลองพบว่าการติดตัวสนับสนุนความปั่นป่วนเพิ่มความเร็วของของไหล และสร้างบริเวณการไหลไม่คงตัว ซึ่งเป็นส่วนสำคัญในการเพิ่มประสิทธิภาพการกรอง ลดการสร้างชั้นเค้กที่ทำให้เกิดการอุดตันของเมมเบรน จากการติดตัวสนับสนุนความปั่นป่วนทั้ง 6 แบบ พบว่าการติดตัวสนับสนุนความปั่นป่วนแบบสี่เหลี่ยมบางมีประสิทธิภาพการกรองมากกว่าการติดตัวสนับสนุนความปั่นป่วนแบบอื่น นอกจากนี้การติดตัวสนับสนุนความปั่นป่วนจะเพิ่มความดันสูญเสียเนื่องจากการเปลี่ยนแปลงการไหลและการเกิดกระแสหมุนวนข้างหลังตัวสนับสนุนความปั่นป่วน แต่อย่างไรก็ตามการเพิ่มขึ้นของความดันตกคร่อมไม่มีความสำคัญเมื่อเทียบกับเพอมิเอทฟลักซ์ (permeate flux)

Thesis Title	Influence of Turbulence Promoter Geometry on Flow Pattern in Cross-Flow Membrane Ultrafiltration
Student	Miss Supawadee Wanthamanee
Student ID.	52611420
Degree	Master of Engineering
Program	Chemical Engineering
Year	2013
Thesis Advisor	Dr.Santi Wattananusorn

ABSTRACT

In this work, the effects of turbulence promoter geometry on flow pattern in cross-flow membrane ultrafiltration were studied. The commercial Computational Fluid Dynamics (CFD) package FLUENT, which employs the finite-volume method, was used for numerical computation. The simulation result was validated by comparing with published experimental data. The simulation models were performed in cross-flow membrane ultrafiltration using six types of turbulence promoters. The results showed that the presence of turbulence promoters cause remarkable increase in the fluid velocity and generate the region of unsteady flow, which can significantly improve the filtration performance and can greatly disrupt the development of cake boundary layer, as well as the growth of fouling. Among the six types of turbulence promoters, the vertical flat-plate shape showed better performances than the others. The presence of turbulence promoters caused the frequent change in flow direction and the eddy formation behind each promoter. The pressure loss and energy cost are increased with eddy formation. However, the increasing in simulated pressure drop is not significant when comparing with permeate flux.

ACKNOWLEDGEMENTS

For my success, I wish to express my sincere thanks to the people who have contributed both directly and indirectly to this study. First of all, I would like to express my appreciation to my research advisor, Dr. Santi Wattananusorn, Department of Chemical Engineering, King Mongkut's Institute of Technology Ladkrabang, for deep discussion and encouraging guidance throughout the course of this work. Furthermore, I would like to thank all members of CFD's Group and my friends for their help, suggestion and warm collaborations. Last but not least, I would like to express my cordial and deep thanks to my family for their encouragement, understanding and huge support.

CONTENTS

Page

Page

Page

LIST OF TABLES

Table Page

LIST OF FIGURES

Figure Page

Figure Page

Figure Page

Figure Page

LIST OF ABBREVIATIONS

C	Inertial resistance factor
$D_{i,m}$	Mass diffusion coefficient for species i in the mixture
E	Total energy
k	Thermal conductivity
L	Total length of membrane in the model
Δn	membrane thickness
p	pressure
Δp	pressure drop
S_E	Total energy source term
S_i	Species source term
S_{Mx}, S_{My}, S_{Mz}	Momentum source term in x, y, z directions
t	Time
T	Temperature
U	Velocity vector
u, v, w	Velocity components in x, y, z directions
x_{tp}	Position on the flow path around turbulence promoter

$x_{total,tp}$	Projected distance from leading edge to trailing edge along turbulence promoter
x, y, z	Rectangular coordinates
α	membrane permeability
μ	Viscosity
ρ	Fluid density
$\tau_{xx}, \tau_{yy}, \tau_{zz}$	Normal stresses on x-x, y-y, z-z planes
$\tau_{xy}, \tau_{xz}, \tau_{yz}$	Shear stresses on x-y, x-z, y-z planes

CHAPTER I
INTRODUCTION

1.1 Background and Motivation

Ultrafiltration (UF) is a separation process using membranes with numerous industrial applications in the purification and separation, such as chemical processing, wastewater handling, drug delivery medium etc., because of its high efficiency and low energy consumed.

However, its performance in many applications is limited by membrane fouling which causes decay in filtrate flux and high cost of membrane filtration process. This phenomenon refers to the deposit of rejected particles of the feed on the surface of the membrane leading to a cake layer building (external fouling) or to adsorption of small particles within the membrane pores (internal fouling). Therefore, to prevent this phenomenon is necessary.

Various techniques controlling membrane fouling have been used to enhance membrane flux, such as applying additional electric fields and ultrasonic fields, the adoption of rotating membranes, membrane surface modification, rapid backflushing pulsing and shocking, feed pretreatment, gas sparging and other methods. Except those techniques, turbulence promoter can be simpler and more effective in overcoming membrane fouling and enhancing membrane flux [1].

Since 1960s, the aerospace industry has integrated Computational Fluid Dynamics (CFD) techniques into design, R&D, and manufacturing of aircraft and jet engines. These methods have been applied to analyze the various fluid flow problems and become an important engineering tool because CFD can produce extremely large volumes of results at virtually low expense to perform parametric studies [2]. CFD is a branch of fluid mechanics that uses numerical method and algorithm to solve and to analyze momentum, heat and mass transfer in various systems. Phenomena of fluid flow are usually explained by three fundamental physical laws, including the conservation of mass, the Newton's second law of

motion, and the first law of thermodynamics. CFD is very useful and spans a wide range of application areas. For example, fluid flow pattern in cyclone separator [3], reactor optimization [4], heat transfer in packed bed column [5] etc.

In recent year, the hydrodynamics analysis and the fluid flow pattern adjacent to the membrane were studied and visualized by computational fluid dynamics (CFD). Cao et al. [6] tested the effects of various arrangements of cylindrical turbulence promoters on fluid flow hydrodynamics. The detailed flow pattern, velocity distributions and turbulence kinetic energy distributions in a spacer filled channel are shown in their study. Significant flux enhancement was achieved using turbulence promoters in a position perpendicular to the flow direction for ultrafiltration of synthetic fruit juice [7]. Rahimi et al. [8] studied a 3D CFD simulation for predicting the water permeate flux through a microfiltration membrane. Pak et al. [9] used a numerical technique to solve the 2D flow field and convective diffusion equation for particle transport in laminar flow over a permeable surface by a tubular membrane. Li Xin et al. [10] showed the effects of promoter geometry on flow pattern.

Regarding to the benefits of CFD and requirement of controlling membrane fouling, a cross-flow membrane ultrafiltration using turbulence promoters to reduce the fouling phenomena has been studied. The flow is assumed to be laminar and incompressible. The effect of different turbulence promoter geometries has been investigated by the CFD modeling and predicted hydrodynamics parameters have been used to explain the observed results.

1.2 Objective of the Research

The objective of this research is to investigate the influence of turbulence promoter geometry on flow pattern in cross-flow membrane ultrafiltration by using FLUENT®.

1.3 Scopes of the Research

1.3.1 Validation of simulation model: comparison between calculated permeate flux result and experimental result

1.3.2 Employ CFD technique using FLUENT® to investigate the influence of turbulence promoter geometry on flow pattern in cross-flow membrane ultrafiltration

- Turbulence promoter geometry, including cylinder, square-bar, diamond, prism type-I, prism type-II and vertical flat-plate

1.4 Procedure of the Research

- Conduct literature survey and review
- Model setup
- Solve problems by using FLUENT®
- Compare simulation results with experiment data which reported in other previous works
- Simulation of turbulence promoter geometry on flow pattern in cross-flow membrane ultrafiltration
- Make discussion and conclusion of simulation results
- Write thesis and preparation of manuscript for journal publication

1.5 Expected Benefit

- Obtain knowledge of influence of turbulence promoter geometry on flow pattern in cross-flow membrane ultrafiltration using FLUENT®.
- This model can be used as a guideline for decreasing membrane fouling in order to obtain the high efficient filtration.

material, such as pectin, polyvinyl alcohol, etc., the amounts of deposited solutes over the membrane surface grows with time and permeate flux declines progressively as the filtration continues as shown in Figure 2.1.

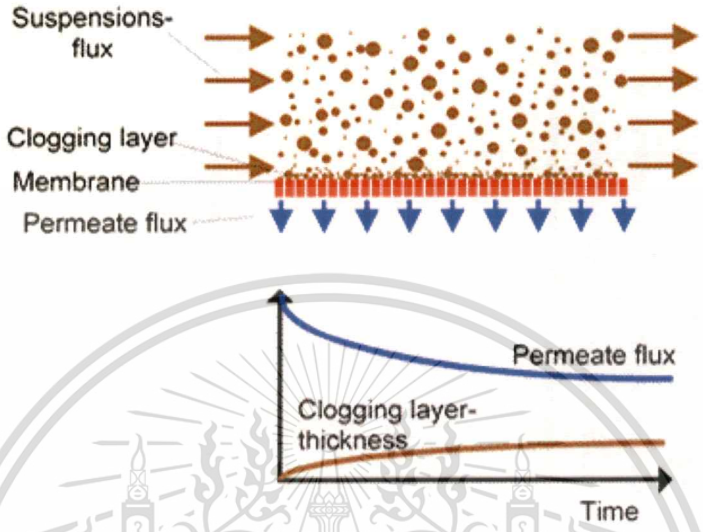

Figure 2.1 Cross-flow filtration [13]

2.2 Computational Fluid Dynamics (CFD)

Computational Fluid Dynamics or CFD is a branch of fluid mechanics that uses numerical technique and algorithm to solve and analyze various flow problems. CFD becomes an important engineering tool because it can provide clear insight into many fluid flow phenomena and produces extremely large volumes of results with inexpensive operating cost. CFD is very powerful and spans a wide range of engineering application areas e.g., aerodynamics of aircraft and vehicles, hydrodynamics of ships, mixing and separation in chemical processes, etc.

2.2.1 CFD processing

Generally, CFD program contains three main processes, including pre-processor, solver, and post-processor [2].

pre-processor

This step consists of the input of flow problem to a CFD program, such as definition of the computational domain, grid generation, selection of the physical and chemical phenomena, definition of material properties, etc.

solver

There are three distinct streams of numerical solution technique, including finite difference method, finite element method, and finite volume methods. Generally, the solver performs the following steps,

- Approximation of unknown flow variables by simple function.
- Transform the PDEs into algebraic equation. This step is called discretisation.
- Solution of the algebraic equations.

post-processor

Post-processor contains versatile data visualization tools, such as geometry and grid display, vector plot, line and shaded contour plots, etc. CFD processing can be summarized as a diagram, shown in Figure 2.2.

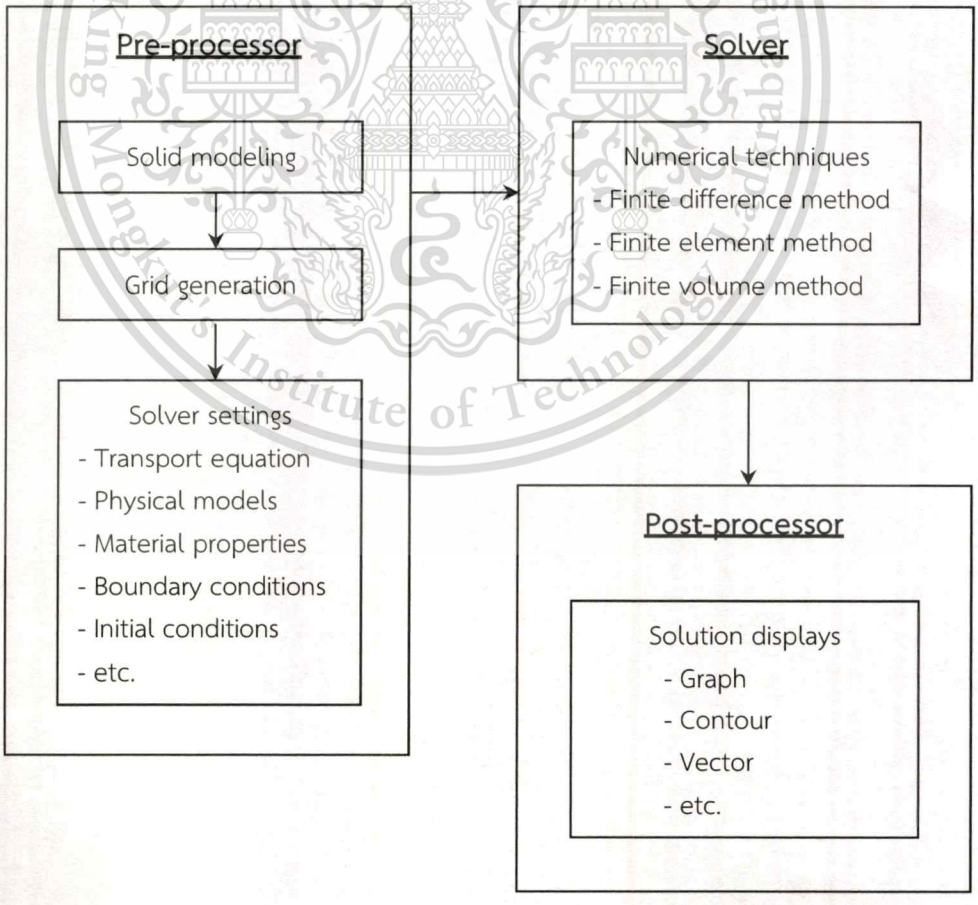

Figure 2.2 CFD processing diagram

2.2.2 Finite volume method

Finite volume method is numerical solution technique. This method was originally developed as a special finite difference formulation. Finite volume method consists of the following steps,

- Integration of fluid flow governing equations over control volume.
- Discretisation involves the substitution of a variety of finite-difference-type approximations in the integrated equation, including convection, diffusion and source terms. This equation converts the integral equations into a set of algebraic equations.
- Solution of the algebraic equations by an iterative method.

2.3 Governing Equations

The fluid problems are usually governed by three fundamental physical equations, including the conservation of mass, the Newton's second law of motion, and the first law of thermodynamics.

2.3.1 Mass conservation equation

The conservation of mass states that mass may be neither created nor destroyed. The mass conservation equation or continuity equation is given by

$$\frac{\partial \rho}{\partial t}+\frac{\partial}{\partial x}(\rho u)+\frac{\partial}{\partial y}(\rho v)+\frac{\partial}{\partial z}(\rho w)=0 \tag{1}$$

or

$$\frac{\partial \rho}{\partial t}+\nabla\cdot(\rho \mathbf{U})=0 \tag{2}$$

where $\mathbf{U}$ is the velocity vector in cartesian coordinate and given by

$$\mathbf{U}=u\,\mathbf{i}+v\,\mathbf{j}+w\mathbf{k}$$

where $\mathbf{i}$, $\mathbf{j}$, and $\mathbf{k}$ are the unit vectors along x, y, and z axes, respectively.

2.3.2 Momentum equations

The Newton's second law of motion states that the rate of change of momentum of a system is equal to the net force acting on the system and takes place in the direction of the net force. The three momentum conservation equations are given by

x-component:

$$\rho\frac{Du}{Dt}=\frac{\partial}{\partial t}(\rho u)+\nabla\cdot(\rho u\mathrm{U})=-\frac{\partial p}{\partial x}+\frac{\partial \tau_{xx}}{\partial x}+\frac{\partial \tau_{yx}}{\partial y}+\frac{\partial \tau_{zx}}{\partial z}+S_{Mx} \tag{3}$$

y-component:

$$\rho\frac{Dv}{Dt}=\frac{\partial}{\partial t}(\rho v)+\nabla\cdot(\rho v\mathrm{U})=-\frac{\partial p}{\partial y}+\frac{\partial \tau_{xy}}{\partial x}+\frac{\partial \tau_{yy}}{\partial y}+\frac{\partial \tau_{zy}}{\partial z}+S_{My} \tag{4}$$

z-component:

$$\rho\frac{Dw}{Dt}=\frac{\partial}{\partial t}(\rho w)+\nabla\cdot(\rho w\mathrm{U})=-\frac{\partial p}{\partial z}+\frac{\partial \tau_{xz}}{\partial x}+\frac{\partial \tau_{yz}}{\partial y}+\frac{\partial \tau_{zz}}{\partial z}+S_{Mz} \tag{5}$$

Equations (1)-(5) are called the compressible Navier-Stokes equations.

2.3.3 Energy equation

The first law of thermodynamics states that if a system is carried through a cycle, the total heat added to the system from its surroundings is proportional to the work done by the system on its surroundings. The energy equation in term of total energy (E) is given by

$$\begin{aligned}\rho\frac{DE}{Dt}=&-\frac{\partial(up)}{\partial x}-\frac{\partial(vp)}{\partial y}-\frac{\partial(wp)}{\partial z}+\frac{\partial}{\partial x}\left(k\frac{\partial T}{\partial x}\right)+\frac{\partial}{\partial y}\left(k\frac{\partial T}{\partial y}\right)+\frac{\partial}{\partial z}\left(k\frac{\partial T}{\partial z}\right)\\&+\frac{\partial(u\tau_{xx})}{\partial x}+\frac{\partial(u\tau_{yx})}{\partial y}+\frac{\partial(u\tau_{zx})}{\partial z}+\frac{\partial(v\tau_{xy})}{\partial x}+\frac{\partial(v\tau_{yy})}{\partial y}+\frac{\partial(v\tau_{zy})}{\partial z}\\&+\frac{\partial(w\tau_{xz})}{\partial x}+\frac{\partial(w\tau_{yz})}{\partial y}+\frac{\partial(w\tau_{zz})}{\partial z}+S_E\end{aligned} \tag{6}$$

2.4 Porous Media Condition [14]

The porous media model can be used for a wide variety of single phase and multiphase problems, including flow through packed beds, filter papers, perforated plates, flow distributors, and tube banks.

Porous media are modeled by the addition of a momentum source term to the standard fluid flow equations. The source term is composed of two parts: a viscous loss term (Darcy, the first term on the right-hand side of Equation 7), and an inertial loss term (the second term on the right-hand side of Equation 7)

$$S_i = -\left(\sum_{j=1}^{3} D_{ij} \mu v_j + \sum_{j=1}^{3} C_{ij} \frac{1}{2} \rho |v| v_j \right) \tag{7}$$

Where S_i is the source term for the *i* th (x, y, or z) momentum equation, $|v|$ is the magnitude of the velocity and D and C are prescribed matrices. This momentum sink contributes to the pressure gradient in the porous cell, creating a pressure drop that is proportional to the fluid velocity (or velocity squared) in the cell.

To recover the case of simple homogeneous porous media

$$S_i = -\left(\frac{\mu}{\alpha} v_i + C_2 \frac{1}{2} \rho |v| v_i \right) \tag{8}$$

where α is the permeability and C_2 is the inertial resistance factor, simply specify D and C as diagonal matrices with $1/\alpha$ and C_2, respectively, on the diagonals (and zero for the other elements).

ANSYS FLUENT also allows the source term to be modeled as a power law of the velocity magnitude:

$$S_i = -C_0 |v|^{C_1} = -C_0 |v|^{(C_1 - 1)} v_i \tag{9}$$

where C_0 and C_1 are user-defined empirical coefficients.

In the power-law model, the pressure drop is isotropic and the units for C_0 are SI.

Darcy's Law in Porous Media

In laminar flows through porous media, the pressure drop is typically proportional to velocity and the constant C_2 can be considered to be zero. Ignoring convective acceleration and diffusion, the porous media model then reduces to Darcy's Law:

$$\nabla p = -\frac{\mu}{\alpha}\vec{v} \tag{10}$$

The pressure drop that ANSYS FLUENT computes in each of the three (x, y, z) coordinate directions within the porous region is then

$$\Delta p_x = \sum_{j=1}^{3} \frac{\mu}{\alpha_{xj}} v_j \Delta n_x$$

$$\Delta p_y = \sum_{j=1}^{3} \frac{\mu}{\alpha_{yj}} v_j \Delta n_y \tag{11}$$

$$\Delta p_z = \sum_{j=1}^{3} \frac{\mu}{\alpha_{zj}} v_j \Delta n_z$$

where $1/\alpha_{ij}$ are the entries in the matrix D in Equation 7, v_j are the velocity components in the x, y, and z directions, and Δn_x, Δn_y and Δn_z are the thicknesses of the medium in the x, y , and z directions.

Inertial Losses in Porous Media

At high flow velocities, the constant C_2 in Equation 7 provides a correction for inertial losses in the porous medium. This constant can be viewed as a loss

coefficient per unit length along the flow direction, thereby allowing the pressure drop to be specified as a function of dynamic head.

Modeling a perforated plate or tube bank can sometimes eliminate the permeability term and use the inertial loss term alone, yielding the following simplified form of the porous media equation:

$$\Delta p = -\sum_{j=1}^{3} C_{2ij}\left(\frac{1}{2}\rho v_j |v|\right) \tag{12}$$

or when written in terms of the pressure drop in the x, y, z directions:

$$\Delta p_x \approx -\sum_{j=1}^{3} C_{2xj}\Delta n_x\left(\frac{1}{2}\rho v_j |v|\right)$$

$$\Delta p_y \approx -\sum_{j=1}^{3} C_{2yj}\Delta n_y\left(\frac{1}{2}\rho v_j |v|\right) \tag{13}$$

$$\Delta p_z \approx -\sum_{j=1}^{3} C_{2zj}\Delta n_z\left(\frac{1}{2}\rho v_j |v|\right)$$

2.5 Separation [15]

Flow passes a curved boundary illustrated in Figure 2.3. The surface is stationary, and the free steam velocity is u_∞. Point A at the nose is where the velocity normal to the surface is zero. This point is referred to as a stagnation point, and the pressure measurement at point A is termed stagnation pressure. The boundary layer begins its growth from here. At points B and C, the boundary layer has experienced a growth that is intuitively predictable. Over the rear portion of the surface, starting at point D, the pressure increase with distance. The fluid particles are slowed down in the boundary layer. The decelerating effect is due to the positive or adverse pressure gradient that has developed. If the decrease in kinetic energy is significant, a region of flow reversal may form. The velocity distribution changes as depicted at point E and F. The velocity at the wall is zero owing to viscosity. At point

D, where separation begins, dV_x/dy is zero at the wall surface. The region of flow reversal is called the separation region because the forward flow has been separated from the boundary by the adverse pressure gradient $dp/dx > 0$. In general, vortices, swirls, reversed flows occur in the separation region.

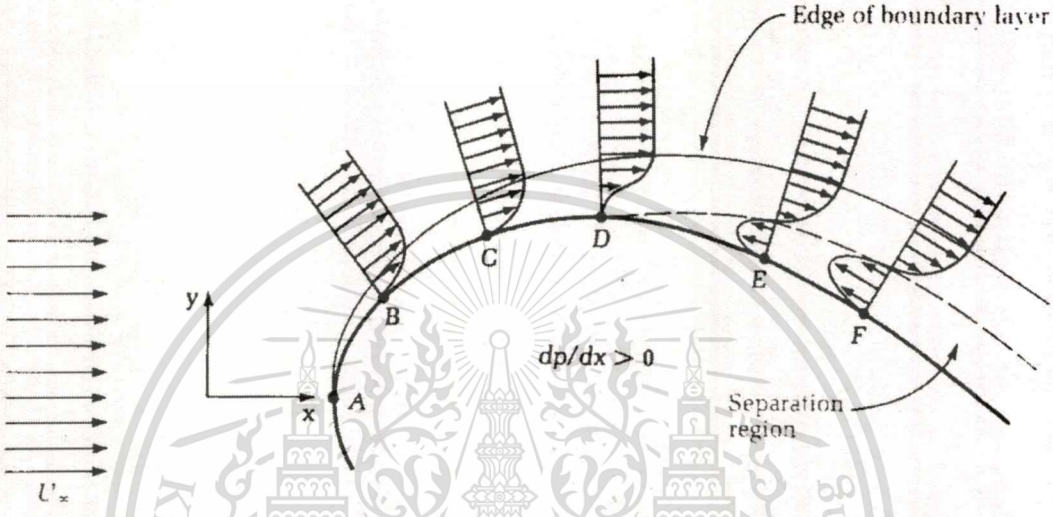

Figure 2.3 Flow past a curved surface

The flow patterns obtained on increasing Re are shown in Figure 2.4.

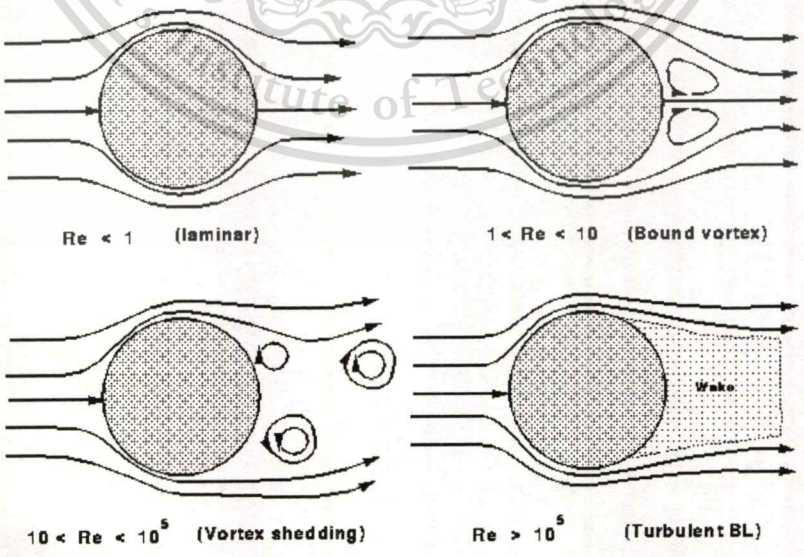

Figure 2.4 Flow pattern for viscous flow past a circular cylinder [16]

2.6 Literature Review

Flux enhancement during ultrafiltration of produced water using turbulence promoter was studied [1]. Experimental investigations were performed on 100 KDa molecular weight cut-off of PVDF single-channel tubular membrane module using four kinds of turbulence promoters. It is observed that the significant flux enhancement in the range of 83%-164% was achieved while the hydraulic dissipated power per unit volume of permeate decreased from 31%-42%, which indicated that the using of turbulence promoter is more efficient than operation without the turbulence promoter.

The effects of various arrangements of turbulence promoters on fluid flow hydrodynamics were studied by Cao et al. [6]. Their CFD simulations revealed the detailed of flow patterns, velocity distributions and turbulent kinetic energy distributions in a spacer-filled channel. They found that the location of the high shear stress region and eddies is closely related to the spacers and their position in the channel. The mass transfer enhancement on the membrane surface was directly related to the high shear stress value, velocity fluctuation, and eddy formation.

Significant flux enhancement was achieved using turbulence promoters in a position perpendicular to the flow direction for ultrafiltration of synthetic fruit juice by R. Bharihoke et al. [7]. The coupled fluid flow and mass transfer processes including the effects of the promoters are modeled and solved using FLUENT. The geometry of the system is constructed using GAMBIT and special attentions are given to mesh sizes in the different zones of flow, e.g., finer mesh is used near the membrane surface. The calculated values of permeate flux under various operating conditions agree well with the experimental data.

Rahimi et al. [8] studied a 3D CFD simulation for predicting the water permeate flux through a microfiltration membrane. The results show that the CFD flux prediction is more accurate in comparison with a simple calculation, in which the average input–output pressures substituted for feed side pressure in the Darcy equation. The effect of transmembrane pressure and fluid mass flow rate on simple

and CFD predictions were investigated. The higher performance of CFD prediction was obtained in lower transmembrane pressures.

Li Xin et al. [10] studied the effects of promoter geometry on flow pattern. The result showed that the strength of flow instability was greater promoted by square bar turbulence promoter than by cylinder turbulence promoter. The reduction of the intersection angle between velocity vector and applied pressure could enhance flow instability, and the effects of the geometries on the flow pattern could be well described by the field synergy principle. It could be concluded that the strength of instabilities was determined not only by velocity but also by the synergy degree between velocity vector and applied pressure. The smaller the intersection angle, the greater was the permeation velocity. The application of field synergy principle might improve membrane process and obtain excellent mass transfer result.

Wiley and Fletcher [17] described the validation and application of a computational fluid dynamics model on pressure driven membrane processes involving selective removal of components in the feed channel and their transfer to the permeate channel. The effects of changes in rejection, wall permeation rates and solution properties on velocity and concentration profiles were presented for empty channels and channels with eddy promoters. They concluded that the region close to the membrane wall needs very fine mesh for high polarization applications, typically in conventional ultrafiltration applications. In addition they reported that high order numerical schemes and accurate modeling of rejection and physical property variations is needed for obtaining accurate and reliable predictions of the polarization and flow phenomenon.

Nong Xu et al. [18] used turbulence promoters with different configurations in ceramic membrane bioreactor. The results confirmed that the introduction of inserts led to better flux in comparison with empty tube. Winding inserts with 10 mm pitch and 1.6 mm wire diameter showed better performances than the others did. The flux under the same operation parameters increased from 70 to 175 L/(mh) and the effluent quality would not reduce in comparison with empty tube.

A detailed study of the performance of helical screw-thread inserts in tubular membranes was carried out [19]. They noted that the screw-thread design generates Dean vortices which promotes good mixing of the fluids and minimizes concentration polarization effects. They found that helical inserts produced much higher fluxes at low cross-flow rates than membranes without inserts (up to a factor higher than 6).

The use of helical baffles in the membrane filtration of baker yeast and dodecane-water emulsion was experimented [20]. A mineral membrane (Carbosep, France) was used. Helical baffles of different number of turns (1, 2, 4, 6) per 25 mm baffle length were made by winding a steel wire (1 mm diameter) on steel rod of 3.1 or 2.3 mm diameter. They reported that under the operating conditions, the use of a helically wound baffle in a membrane managed to increase the permeate flux, in some cases up to more than 50% at the same hydraulic dissipated power and without any additional equipment such as pulsating pump or any backwashing system.

Krsti et al. [21] demonstrated that use of a static mixer as turbulence promoter results in enhanced cross-flow microfiltration of skim milk. Experimental investigations were performed on 50 nm and 100 nm ceramic tubular membranes. The use of a static mixer provided a significant reduction of membrane fouling and an increase of more than 700% in permeate flux for both membranes compared with that obtained without a static mixer at the-same feed flow rate. The similar flux enhancement indicates that surface layer resistance dominates the overall fouling resistance.

CHAPTER III
SIMULATION

Procedures of simulation are described in this chapter. This simulation research is based on the experimental work of experimental and theoretical analysis of turbulence promoter assisted ultrafiltration of synthetic fruit juice by S. Pal et al. [7]. Based on our literature survey, the following simulation procedures are designed as a tentative guideline. Simulation works are separated into 3 parts; (i) model setup, (ii) validation of the model, and (iii) simulation of turbulence promoter in cross-flow membrane ultrafiltration.

3.1 Model Setup

3.1.1 Modeling of turbulence promoter in cross-flow membrane ultrafiltration

This simulation were set up based on the experimental work which reported by S. Pal et al. [7]. The cross flow ultrafiltration system is a rectangular cross flow chamber, made of two matching flanges of stainless steel is fabricated. The effective channel height after tightening the two flanges with gaskets in between is 0.0034 m. The membrane area available for filtration is 0.012 m^2 with a length of 0.26 m and a width of 0.0455 m. The promoters are positioned in between the two gaskets as shown in Figure 3.1 Stainless steel wires with cross-sectional diameter of 1.68×10^{-3} m are used as promoters.

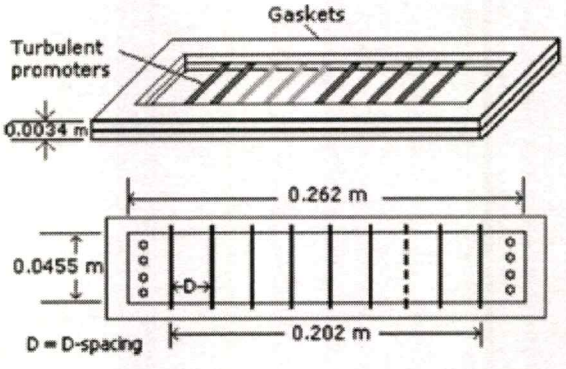

Figure 3.1 Model scheme of the flow channel used for validation [7]

This cross flow ultrafiltration system was simplified to be two-dimensional as shown in Figure 3.2. The calculation domain and grid generation was done by GAMBIT as shown in Figure 3.3. Simulations with two promoters show that the flow field keeps on repeating itself when additional promoters are added and therefore two promoters are shown in subsequent figures for clarity. However, the flux values are calculated taking into consideration the effects of all the promoters present in the flow path. The relevant values of the geometric parameters are as follows: height of the channel is 3.4×10^{-3} m, projected length of promoter is 1.68×10^{-3} m and spacing between consecutive promoters is 14.4×10^{-3} m. The grids are uniform in the region encompassing the promoter and the non-permeable upper wall of the channel. In the lower part, (from below the promoter to the membrane surface) the grid spacing decreases linearly and is smallest near the membrane surface.

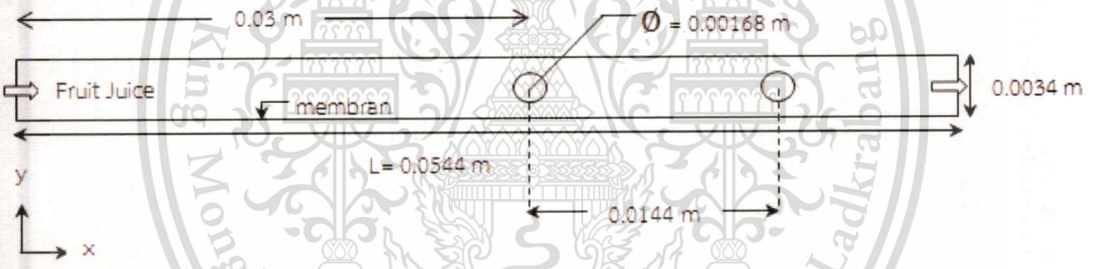

Figure 3.2 Calculation domain

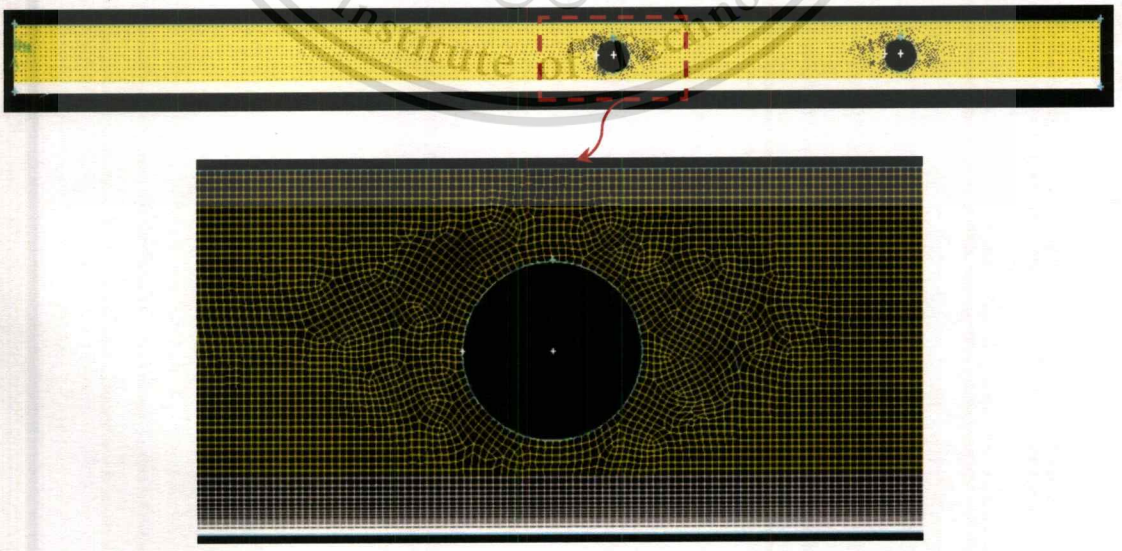

Figure 3.3 Grid generation of calculation domain

3.1.2 Boundary conditions

The boundary condition for fruit juice velocity at the inlet was assumed to be uniform flow (Re = 615.29). The pressure-outlet boundary condition was used at the exit. At the wall, no-slip boundary condition was applied. About 55,000 quad cells were employed to obtain grid independent solution. The numerical results were carried out with the residuals less than 10^{-4}.

3.1.3 Assumptions of the model

- The model was simplified to be two-dimensional flow.
- The flow was assumed to be laminar.
- Fruit juice was considered to be incompressible fluid.

3.1.4 Governing equations of the model

According to the assumptions of the model, the governing equations of the model, including continuity equation, momentum equations, can be expressed as follows,

continuity equation:

$$\frac{\partial v_x}{\partial x} + \frac{\partial v_y}{\partial y} = 0 \tag{14}$$

momentum equation in x-direction:

$$\rho v_x \frac{\partial v_x}{\partial x} + \rho v_x \frac{\partial v_y}{\partial y} = -\frac{\partial p}{\partial x} + \mu\left(\frac{\partial^2 v_x}{\partial x^2} + \frac{\partial^2 v_x}{\partial y^2}\right) + S_{Mx} \tag{15}$$

momentum equation in y-direction:

$$\rho v_y \frac{\partial v_x}{\partial x} + \rho v_y \frac{\partial v_y}{\partial y} = -\frac{\partial p}{\partial y} + \mu\left(\frac{\partial^2 v_y}{\partial x^2} + \frac{\partial^2 v_y}{\partial y^2}\right) + S_{My} \tag{16}$$

porous media:

$$S_i = -\left(\frac{\mu}{\alpha} v_i + C\frac{1}{2}\rho|v|v_i\right) \tag{17}$$

pressure drop in x-direction:

$$\Delta p_x = \sum_{i=1}^{2} \frac{\mu}{\alpha_{xi}} v_i \Delta n_x \tag{18}$$

pressure drop in y-direction:

$$\Delta p_y = \sum_{i=1}^{2} \frac{\mu}{\alpha_{yi}} v_i \Delta n_y \tag{19}$$

transmembrane pressure in y-direction:

$$\Delta p_y = \frac{\mu}{\alpha} v_y \Delta n_y \tag{20}$$

3.1.5 Numerical methods

Governing equations have been solved numerically by using FLUENT® with Finite Volume Method (FVM), in which the computation domain is divided into a number of small cells, and the partial differential equations are integrated over each cell to obtain a set of algebraic equations. These algebraic equations were solved iteratively to obtain the field distribution of dependent variables. For this study, the pressure-velocity coupling was solved by using SIMPLE algorithm. The spatial discretization of gradient and pressure were least squares cell based and standard, respectively. Second order upwind scheme was applied to calculate momentum as shown in Table 3.1.

CHAPTER II
THEORY AND LITERATURE REVIEW

2.1 Ultrafiltration Membrane [11, 12]

Separation and purification processes using membrane technology are gaining popularity in many chemical and food processing as well as in waste treating industries. The technology offers several advantages over and above the traditional techniques, including low energy requirement and low temperature of operation.

Cross-flow ultrafiltration is a pressure driven process for separating macromolecules smaller than about 100,000 Da in size. Typical hydrostatic pressure of 60–600 kPa applies across the membrane. The feed flow is tangential to the surface of membrane. The solvent is forced through the membrane as permeate. Solutes that are unable to pass through are retained, concentrated and removed tangential to the membrane surface as retentate. Flux of a membrane is defined as the amount of permeate produced per unit area of membrane surface per unit time.

The major problem in membrane separation process is decline in flux over time of operation. This flux decline is attributed to the fouling of membrane. Membrane fouling is affected by three major factors, namely, the membrane material properties, the feed characteristics and the operating parameters. There are two type of membrane fouling, i.e., reversible and irreversible fouling. Reversible fouling is mainly caused by a phenomenon, known as concentration polarization. Concentration polarization is the accumulation of solute particles over the membrane surface. This phenomenon is predominantly a function of membrane channel hydrodynamics. In case of reversible fouling, the membrane permeability is recovered significantly after a proper washing protocol. The concentration polarization can facilitate irreversible fouling of membrane by altering interactions among solvent, solute and membrane. Adsorption of solute in the membrane pores causing partial or complete blocking is the original cause of irreversible fouling and the membrane permeability is permanently lost to some extent even after proper cleaning. In case of a gel forming

Table 3.1 Solution methods

Solution Methods	
Pressure-Velocity Coupling	SIMPLE
Gradient	Least Squares Cell Based
Pressure	Standard
Momentum	Second Order Upwind

3.2 Validation of the Model

Validation can be defined as a process for assessing simulation modeling uncertainty by using benchmark experimental data [22]. The simulation permeate flux result of cylinder promoter was validated by comparing with experimental result which reported by S. Pal et al. [7].

3.3 Simulation of Turbulence Promoter in Cross-Flow Membrane Ultrafiltration

Six types of turbulence promoters were used. Geometries of the promoter were shown in Figure 3.4.

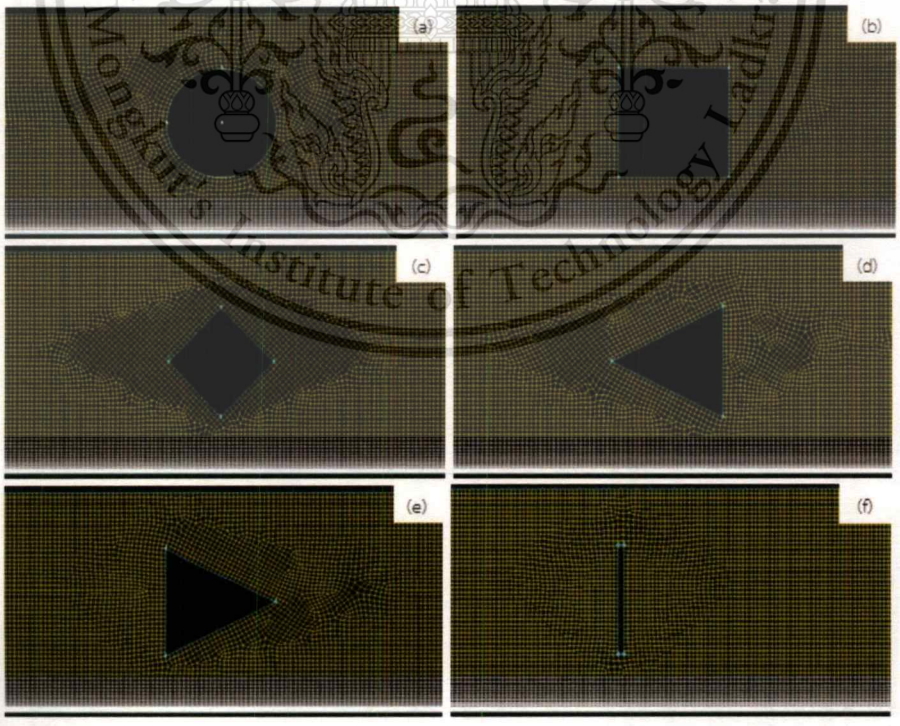

Figure 3.4 Geometries of turbulence promoter: (a) cylinder (b) square–bar (c) diamond (d) prism type-I (e) prism type-II (f) vertical flat-plate

CHAPTER IV
RESULTS AND DISCUSSION

4.1 Validation of the Model

In order to verify CFD simulations, the cross-flow ultrafiltration of fruit juice were conducted with inlet velocity of 0.16 m/s and outlet pressure of 350 kPa. The size of membrane and geometric parameters of cylinder promoters are identical as those depicted in [7]. The variation between the experimental and calculated value of permeate flux are 3.80% as shown in Table 4.1.

Table 4.1 The variation between the experimental and calculated value of permeate flux

Promoter Geometry	Permeate Flux x 10^6 (m^3/m^2s)		Error (%)
	Experiment	Simulation	
Cylinder	7.11	6.84	3.80

4.2 The Effect of Turbulence Promoter Geometry

The x-velocity contours in case of using various turbulence promoter geometries are shown in Figure 4.1. The particles in the feed solution are prone to deposit on the membrane surface to form a thick cake layer, resulting in the decline of filtration flux which defines as volumetric flow rate through the membrane per its area. Fortunately, the presence of turbulence promoter not only localized turbulence around the promoters, but also interrupts development of the boundary layer on the membrane surface. Both aforementioned effects tend to reduce membrane fouling and consequently improve the performance of membrane. A conceptual view of the change in deposition thickness around a cylinder turbulence promoter, placed perpendicularly in the flow path, is presented in Figure 4.2 As the feed solution flows tangentially over the membrane surface, it encounters the promoters and flows around them through the gap between the promoters and the top and bottom (membrane) surfaces.

The cake buildup reduces permeate flux. When the turbulence promoter is inserted into membrane channel, fluid flow pattern are changed. The turbulence promoters increase the shear rate at the membrane surface which results in membrane surface scouring, more than the systems without turbulence promoters. This increased scouring of the membrane surface leads to the decrease in cake layer thickness resulting in increased flux values.

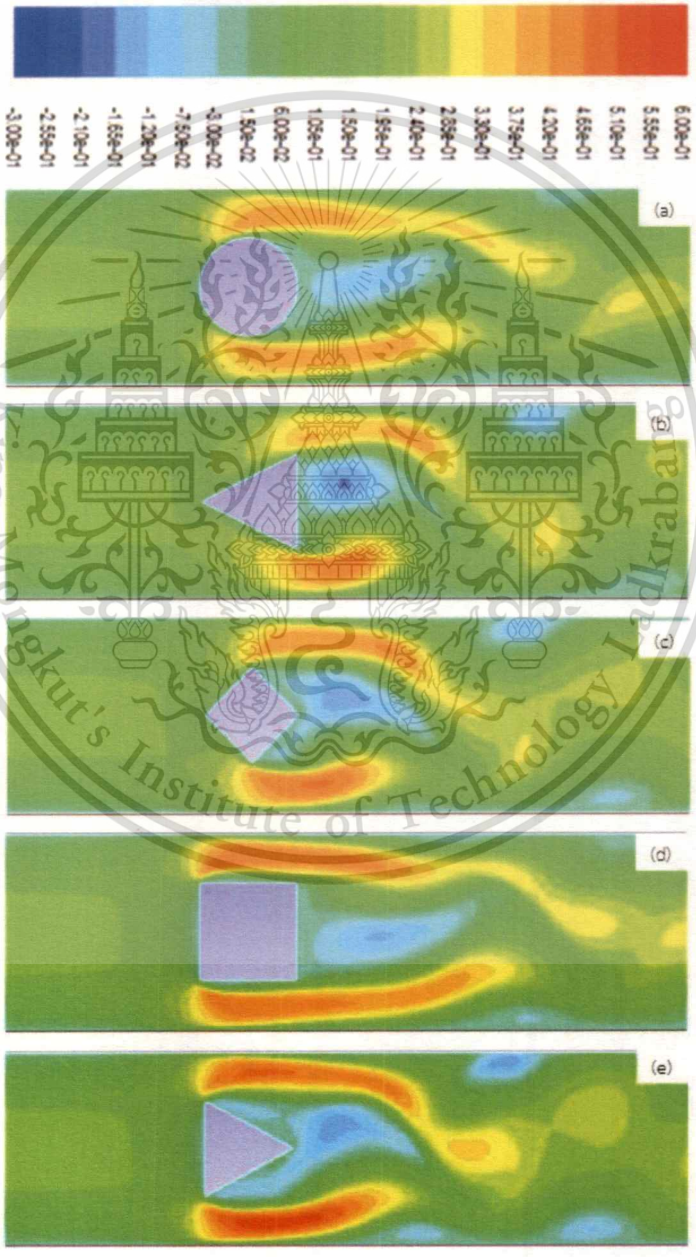

Figure 4.1 The x-velocity contours (m/s) around turbulence promoter: (a) cylinder (b) prism type-I (c) diamond (d) square–bar (e) prism type-II

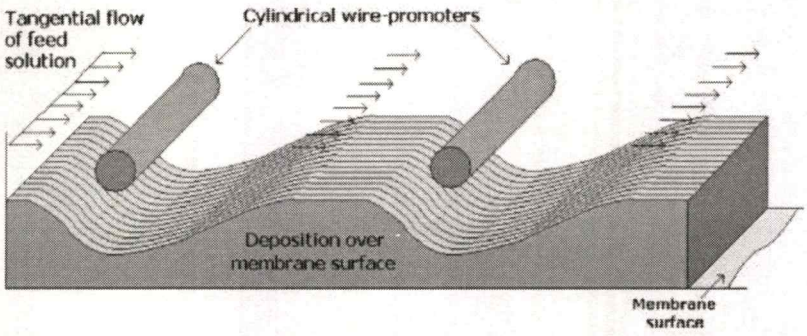

Figure 4.2 Conceptual view of the effect of turbulence promoters on flow and deposition [7].

The shape of prism type-II produces the highest x-velocity under the promoters as shown in Figure 4.1 (e), the permeate flux should be the highest. Therefore, all y-velocites were plotted and integrated in order to confirm the model results, as shown in Figure 4.3 and Table 4.2, respectively. The velocity fluctuations for different turbulence promoters are presented in Figure 4.3. It suggests that the presence of turbulence promoters causes a periodical appearance of trough and peak value of velocity. From the channel inlet, the fluid flow gradually slows down before the first turbulence, reaching its trough value in the middle of turbulence promoter interval, and then it sharply accelerates and reaches its peak value in the position where each turbulence promoter is located. After passing the first turbulence promoter, it decreases and reaches its trough value again. Then the above phenomena are repeated for the following the turbulence promoter.

The results show that the prism type-II turbulence promoter can produce numerous y-velocities. Table 4.2 clearly shows that for all simulations with the turbulence promoter, the flux is always higher than the simulation without any turbulence promoter. This results prove that the presence of turbulence promoter reduces membrane fouling thus increases the permeate flux.

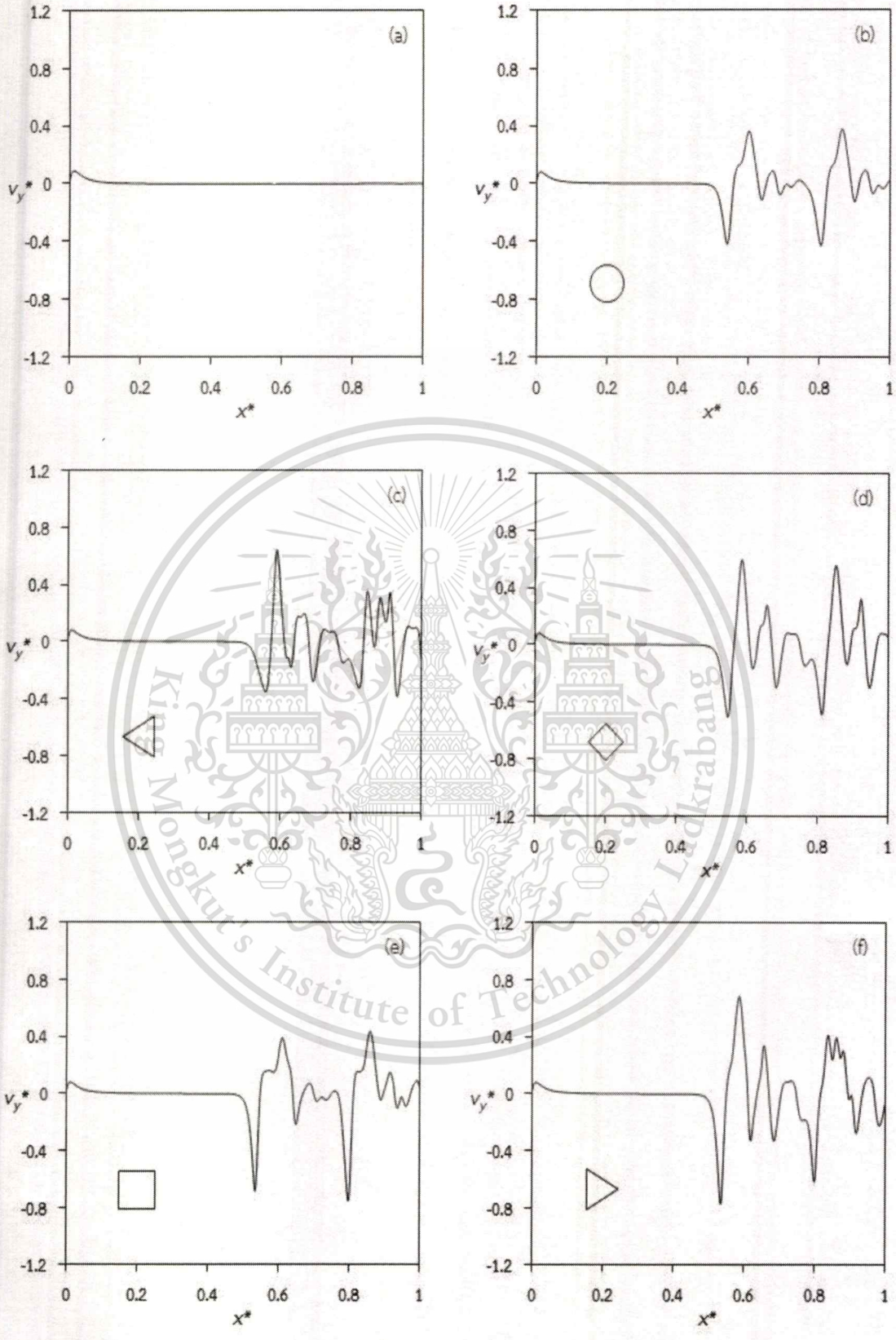

Figure 4.3 The y-velocity underneath turbulence promoters: (a) without (b) cylinder (c) prism type-I (d) diamond (e) square–bar (f) prism type-II where $v_y^* = v_y/v_{inlet}$ and $x^* = x/L$

Figure 4.4 depicts the velocity distribution pass a surface from leading edge to trailing edge of various the first turbulence promoters. In the area near the stagnation point where the velocity normal to the surface is zero, It is found that the velocity of the blunt body (cylinder turbulence promoter) and the block body (square and prism type-II turbulence promoter) and the sharp body (diamond and prism type-I turbulence promoter) near zero. The separation point where the velocity change the sign from positive to negative of the cylinder turbulence promoter occurred at x_{tp}^* = 0.7, as for the prism type-I occurred at x_{tp}^* = 1.0 but permeate flux of prism type-I turbulence promoter is more than cylinder turbulence promoter. The square-bar and prism type-II turbulence promoter occur the same separation point but the reattachment point of the prism type-II turbulence promoter occurred further, hence increasing eddy region and resulting in the highest permeate flux.

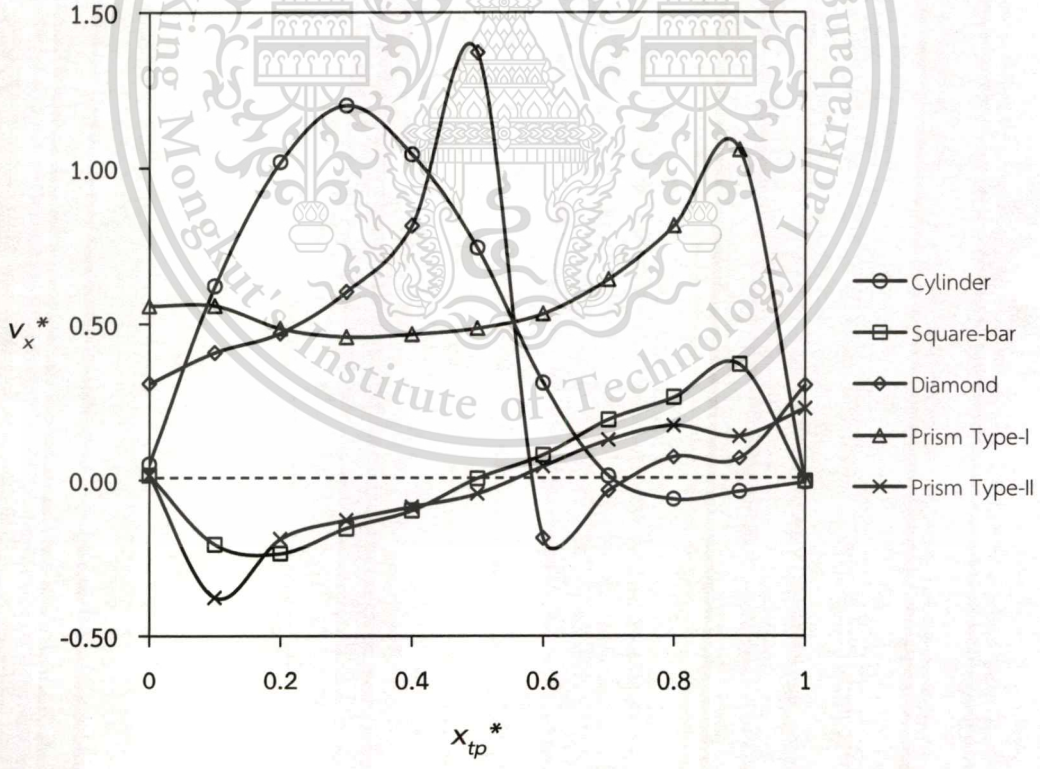

Figure 4.4 Velocity distributions along lower surface of various turbulence promoter where $v_x^* = v_x/v_{inlet}$ and $x_{tp}^* = x_{tp} / x_{total,tp}$

The static pressure distributions in the flow path are shown in Figure 4.5. For five cases (Figures 4.5 (b) – (d)), when the fluid passes each promoter, it always undergoes a sudden drop of static pressure, corresponding to the velocity fluctuation and eddy formation. From Figure 4.5, the pressure drop across the turbulence promoter, the difference of static pressures between x = 0.0228 m and x = 0.0372 m (inlet x = 0), can be obtained. At an inlet velocity of 0.16 m/s and outlet pressure of 350 kPa, the pressure drop across the turbulence promoter is about 46.75, 64.44, 61.13, 71.09 and 83.75 Pa for the cylinder, prism type-I, diamond, square-bar and prism type-II promoter, respectively, which is much higher than that for without promoter (5.44 Pa). The pressure drop leads to the increase in additional energy cost of the membrane module. There are two main reasons accounting for the pressure drop across the membrane channel. Firstly, the presence of turbulence promoter causes the frequent change in the flow direction and intense velocity fluctuation, which will increase the frictional loss of the fluid flow. Secondly, the eddy formed behind promoters also results in the increase of energy loss.

Table 4.2 Performances of membrane with different types of turbulence promoter

Promoter Geometry	Permeate Flux x 10^6 ($m^3/m^2 s$)	Pressure Drop (Pa)	Separation Point (-)
Without	1.14	5.44	-
Cylinder	6.84	46.75	0.7
Prism Type-I	8.33	64.44	1
Diamond	8.86	61.13	0.57
Square-bar	9.50	71.09	0
Prism Type-II	11.83	83.75	0

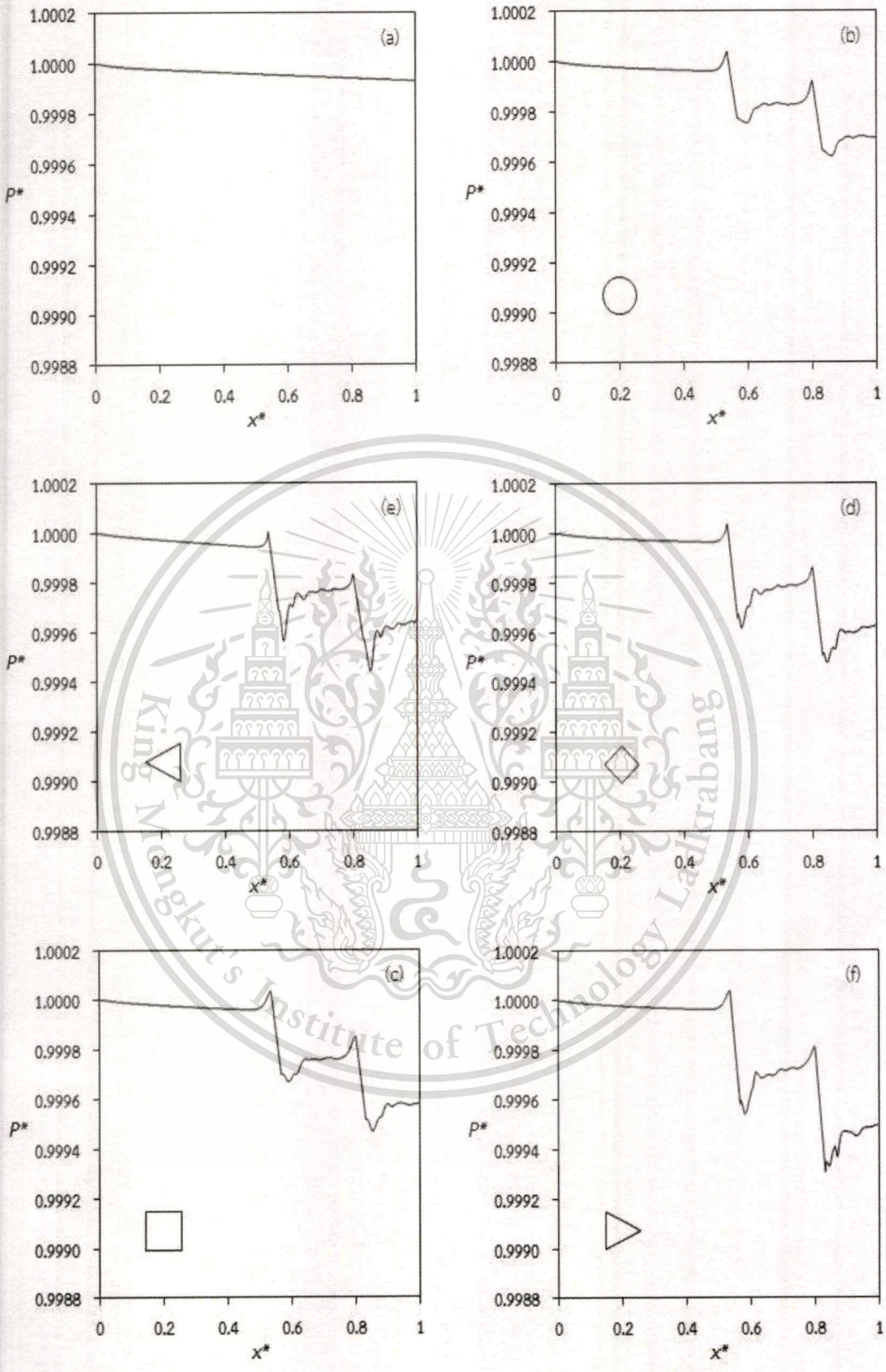

Figure 4.5 Static pressure distributions in the flow path: (a) without (b) cylinder (c) square–bar (d) diamond (e) prism type-I (f) prism type-II where $P^* = P/P_{inlet}$

From x-velocity contour of square and prism type-II turbulence promoter in Figures 4.1 (d) and (e), it is found that eddy region of prism type-II turbulence promoter occur more than square turbulence promoter resulting the largest the permeate flux. According to these results, it observes the shape where fluid encounter is the same but the area behind the turbulence promoter is different that prism type-II turbulence promoter less than square turbulence promoter thus a new turbulence promoter is vertical flat-plate. As the fluid past the edges of flat-plate turbulence promoter, eddy are generated caused increase velocity as shown in Figures 4.6 (c) and 4.7 (c) leading to scouring of the membrane surface more than in the case of the square-bar and prism type-II. The enhanced scouring in the turbulence promoter mode of operation remove particles from the surface and reduces the fouling of the particles deposit on the membrane surface, which leading to a large improvement of the permeate flux.

The static pressure distributions of flat-plate turbulence promoters are shown in Figure 4.8. When the fluid passes each promoter, it always undergoes a sudden drop of static pressure as the same trend the others turbulence promoters but pressure drop value is more than all studied geometries corresponding to the velocity fluctuation and eddy formation. The simulated permeate flux and pressure drop of vertical flat-plate are 14.67 m^3/m^2s and 88.78 Pa, respectively as shown in Table 4.3.

Table 4.3 Performances of membrane with three types of turbulence promoter

Promoter Geometry	Permeate Flux x 10^6 (m^3/m^2s)	Pressure Drop (Pa)
Square-bar	9.50	71.09
Prism Type-II	11.83	83.75
Vertical flat-plate	14.67	88.78

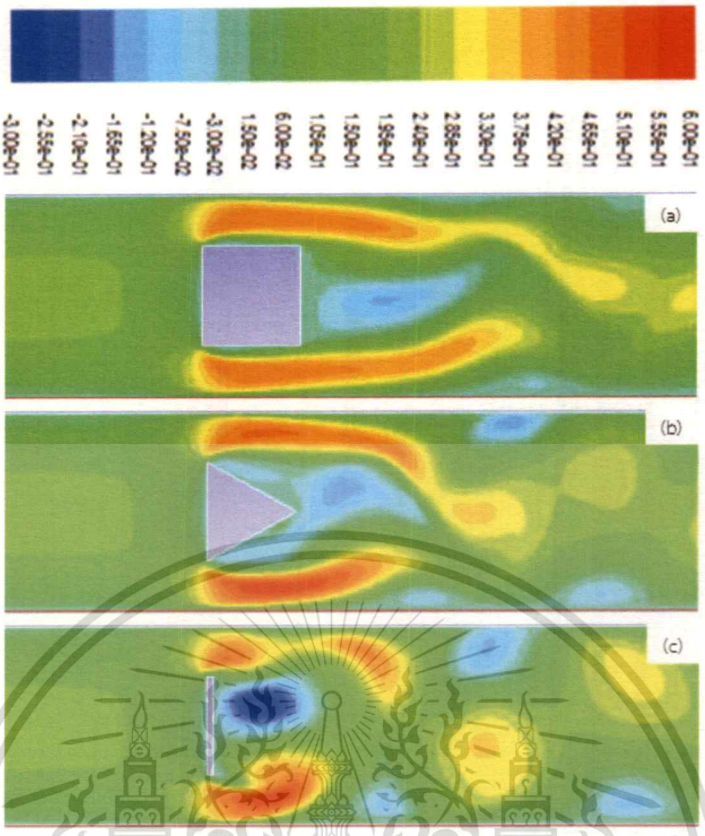

Figure 4.6 The x-velocity contours (m/s) around three types turbulence promoter: (a) square-bar (b) prism type-II (C) vertical flat-plate

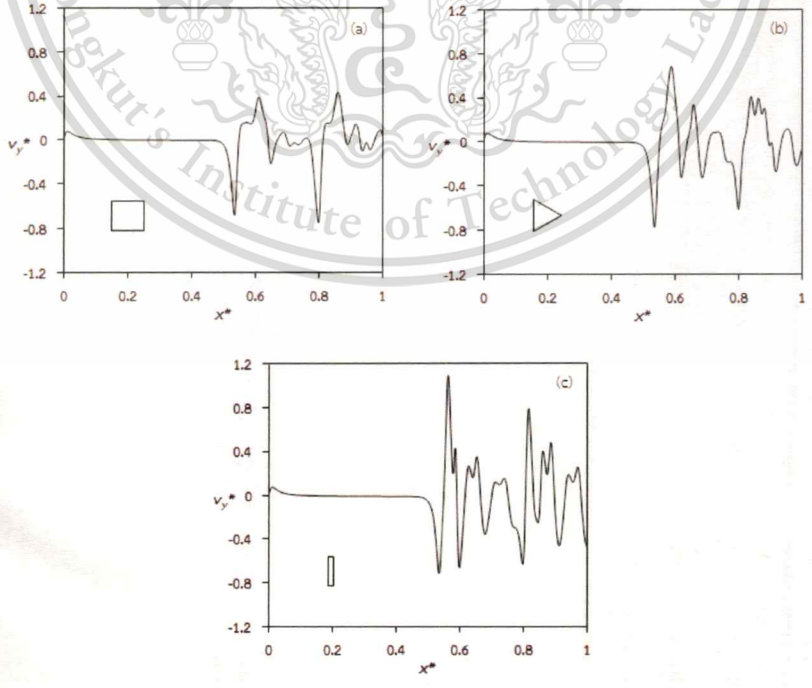

Figure 4.7 The y-velocity underneath three types turbulence promoters: (a) square-bar (b) prism type-II (C) vertical flat-plate where $v_y^* = v_y/v_{inlet}$ and $x^* = x/L$

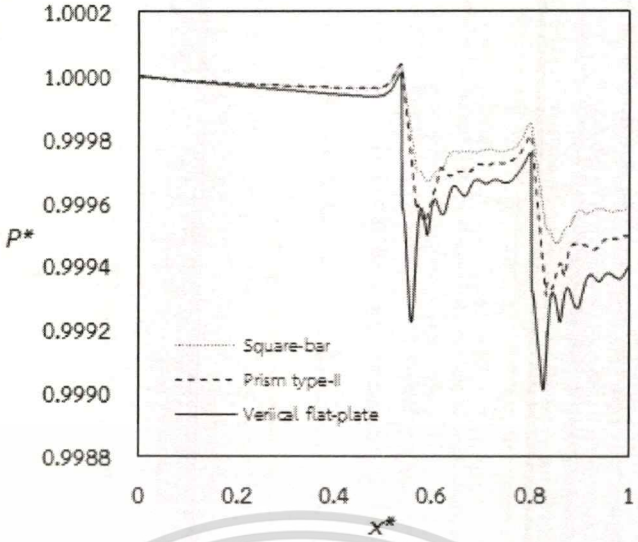

Figure 4.8 Comparison among the static pressure distributions for three types turbulence promoters in the flow path where $P^* = P/P_{inlet.}$

CHAPTER V
CONCLUSIONS AND RECOMMENDATIONS

5.1 Conclusions

In this work, Turbulence Promoter in Cross-Flow Membrane Ultrafiltration was investigated using a CFD program, FLUENT®. The study focused on the effects of turbulence promoter geometries. The simulation boundary conditions were set up based on the experimental work of S. Pal et al. [7]. The model was simplified to be two dimensional model. The motion of fruit juice was considered to be incompressible laminar flow.

The effect of different turbulence promoter geometries has been explored. The simulation results clearly showed that the improved performance of cross-flow membrane ultrafiltration can be obtained by using the turbulence promoter. The insertion of turbulence promoter caused a large improvement of the permeate flux and the vertical flat-plate turbulence promoter leads to the largest improvement of the permeate flux with among the six types of turbulence promoters. To obtain the maximum filtration performance, flat plate turbulence promoter is recommended. Comparing the system with flat plate turbulence promoter with no turbulence promoter, the average flux can be enhanced up by a factor of 12.83. The presence of turbulence promoters caused the frequent changes in flow direction and the eddy formation behind each promoter, which increased the pressure losses and energy costs. However, the increase in pressure drop is insignificant.

5.2 Recommendations

1. Use three dimensional simulation instead of two dimensional simulation to eliminate the error resulting from two dimensional model.

2. The simulation may be extended to study the various size and the others shape of the turbulence promoter in order to find the higher performances of membrane.

REFERENCES

[1] Xiang-hua Z., Shui-li Y., Bei-h W., Hai-feng Z. "Flux enhancement during ultrafiltration of produced water using turbulence promoter." **Journal of Environmental Sciences**, vol. 18, 2006. pp. 1077-1081

[2] Versteeg H. Malalasekera K., W. **An introduction to computational fluid dynamics The finite volume method**. Malaysia : Prentice Hall. 1995.

[3] Kaya F., Karagoz I. "Numerical investigation of performance characteristics of a cyclone prolonged with a dipleg." **Chemical Engineering Journal**, vol. 151, 2009. pp. 39-45

[4] Reuge N., Bacsa R., Serp P., Caussat B. "Chemical Vapor Synthesis of Zinc Oxide Nanoparticles: Experimental and Preliminary Modeling Studies." **Journal of Physical Chemistry**, vol. 113, 2009. pp. 19845-19852

[5] Nijemeisland M., Dixon A. G. "Comparison of CFD simulations to experiment for convective heat transfer in a gas–solid fixed bed." **Chemical Engineering Journal**, vol. 82, 2001. pp. 231-246

[6] Cao Z., Wiley D.E., Fane A.G. "CFD simulation of net-type turbulence promoters in narrow channel." **Journal of Environmental Sciences**, vol. 185, 2001. pp. 157-176

[7] Pal S., Bharihoke R., Chakraborty S., Ghatak S. K., De S., DasGupta S. "An experimental and theoretical analysis of turbulence promoter assisted ultra-filtration of synthetic fruit juice." **Separation and Purification Technology**, vol. 62, 2008. pp. 659-667

[8] Rahimi M., Madaeni S. S., Abbasi K. "CFD modeling of permeate flux in cross-flow microfiltration membrane." **Journal of Membrane Science**, vol. 255, 2005. pp. 23-31

[9] Pak A., Mohammadi T., Hosseinalipour S. M., Allahdini V. "CFD modeling of porous membranes." **Desalination**, Vol. 222, 2008. pp. 482-488

[10] LiXin L., Xinping P., Jiong S. Yi. "Comparison of turbulence promoter geometry on flow pattern from view point of field synergy principle." **Procedia Environmental Sciences**, vol. 11, 2011. pp. 1566-1573

[11] Cheryan M. **Ultrafiltration Handbook**. Pennsylvania : Technomic. 1986.

[12] Baker R. W. **Membrane Technology and Applications.** England : Wiley. 2004.

[13] "Cross-flow Filtration" [Online]. Available: http://www.springerimages.com

[14] ANSYS, Inc. ANSYS FLUENT 12.0 User's Guide. 2008.

[15] Janna W. S. **Introduction to Fluid Mechanics.** Boston : PWS. 1993.

[16] "Separation flow" [Online]. Available: http://www.see.ed.ac.uk

[17] Wiley D.E., Fletcher D.F. "Computational fluid dynamics modelling of flow and permeation for pressure-driven membrane processes." **Desalination**, vol. 145, 2002. pp. 183-186

[18] Xu N., Xing W., Shi J. "Application of turbulence promoters in ceramic membrane bioreactor used for municipal wastewater reclamation." **Journal of Membrane Science**, vol. 210, 2002. pp. 307–313

[19] Bellhouse B. J., Costigan G., Abinava K., Merry A. "The performance of helical-screw-thread inserts in tubular membranes." **Separation and Purification Technology**, vol. 22-23, 2001. pp. 89-113

[20] Gupta B. B., Howell J. A., Wu D., Field R. W. "A helical baffle for cross-flow microfiltration." **Journal of Membrane Science**, vol. 99, 1995. pp. 31-42

[21] Krsti D. M., Tekic M. N., Cari M. D., Milanovi S. D. "Kenics static mixer as turbulence promoter in cross-flow microfiltration of skim milk." **Separation and Purification Technology**, vol. 38, 2003. pp. 1549-1560

[22] Stern F., Wilson R. V., Coleman H. W., Paterson E. G. **VERIFICATION AND VALIDATION OF CFD SIMULATIONS.** IIHR Report No. 407. Iowa : Iowa Institute of Hydraulic Research. 1999.

APPENDICES

APPENDIX A
SIMPLE ALGORITHM

SIMPLE stands for Semi Implicit Method for Pressure-linked Equations. This algorithm was introduced by Patankar and Spalding (1972) [2]. This method can be demonstrated by two-dimensional laminar steady flow equations in Cartesian co-ordinates.

$$a_{i,J}u_{i,J} = \sum a_{nb}u_{nb} + \left(p_{I-1,J} - p_{I,J}\right)A_{i,J} + b_{i,J} \tag{A-1}$$

$$a_{I,j}v_{I,j} = \sum a_{nb}v_{nb} + \left(p_{I,J-1} - p_{I,J}\right)A_{I,j} + b_{I,j} \tag{A-2}$$

First, the pressure field p^* (guessed pressure) is guessed. Then, substituting p^* into equations (A-1) and (A-2) to yield u^* and v^* as follows

$$a_{i,J}u^*_{i,J} = \sum a_{nb}u^*_{nb} + \left(p^*_{I-1,J} - p^*_{I,J}\right)A_{i,J} + b_{i,J} \tag{A-3}$$

$$a_{I,j}v^*_{I,j} = \sum a_{nb}v^*_{nb} + \left(p^*_{I,J-1} - p^*_{I,J}\right)A_{I,j} + b_{I,j} \tag{A-4}$$

Then, the pressure correction and velocities correction can be defined as follows

$$p' = p - p^* \tag{A-5a}$$

$$u' = u - u^* \tag{A-5b}$$

$$v' = v - v^* \tag{A-5c}$$

Subtraction equations (A-3) and (A-4) from equations (A-1) and (A-2), respectively. Then, using correction formulae equations (C-5a)-(C-5c) to yield equations (A-6) and (A-7).

$$a_{i,J}u'_{i,J} = \sum a_{nb}u'_{nb} + \left(p'_{I-1,J} - p'_{I,J}\right)A_{i,J} \tag{A-6}$$

$$a_{I,j}v'_{I,j} = \sum a_{nb}v'_{nb} + \left(p'_{I,J-1} - p'_{I,J}\right)A_{I,j} \tag{A-7}$$

Approximating equations (A-6) and (A-7) by eliminate $\sum a_{nb}u'_{nb}$ and $\sum a_{nb}v'_{nb}$. Equations (A-6) and (A-7) become

$$u'_{i,J} = d_{i,J}\left(p'_{I-1,J} - p'_{I,J}\right) \tag{A-8}$$

$$v'_{I,j} = d_{I,j}\left(p'_{I,J-1} - p'_{I,J}\right) \tag{A-9}$$

where $d_{i,J} = \dfrac{A_{i,J}}{a_{i,J}}$ and $d_{I,j} = \dfrac{A_{I,j}}{a_{I,j}}$

Substituting equations (A-8) and (A-9) into equations (A-5b) and (A-5c), respectively. Then, rearranging the results to yield equations (A-10) and (A-11).

$$u_{i,J} = u^*_{i,J} + d_{i,J}\left(p'_{I-1,J} - p'_{I,J}\right) \tag{A-10}$$

$$v_{I,j} = v^*_{I,j} + d_{I,j}\left(p'_{I,J-1} - p'_{I,J}\right) \tag{A-11}$$

Similar expressions exist for $u_{i+1,J}$ and $v_{I,j+1}$:

$$u_{i+1,J} = u^*_{i+1,J} + d_{i+1,J}\left(p'_{I,J} - p'_{I+1,J}\right) \tag{A-12}$$

$$v_{I,j+1} = v^*_{I,j+1} + d_{I,j+1}\left(p'_{I,J} - p'_{I,J+1}\right) \tag{A-13}$$

where $d_{i+1,J} = \dfrac{A_{i+1,J}}{a_{i+1,J}}$ and $d_{I,j+1} = \dfrac{A_{I,j+1}}{a_{I,j+1}}$

The velocity field will satisfy continuity equation. The discretised continuity equation is given by

$$\left((\rho uA)_{i+1,J} - (\rho uA)_{i,J}\right) + \left((\rho vA)_{I,j+1} - (\rho vA)_{I,j}\right) = 0 \tag{A-14}$$

Substituting the corrected velocity into equation (A-14) yields the pressure correction equation.

$$a_{I,J}p'_{I,J} = a_{I+1,J}p'_{I+1,J} + a_{I-1,J}p'_{I-1,J} + a_{I,J+1}p'_{I,J+1} + a_{I,J-1}p'_{I,J-1} + b'_{I,J} \tag{A-15}$$

where $a_{I,J} = a_{I+1,J} + a_{I-1,J} + a_{I,J+1} + a_{I,J-1}$ and the coefficients are given in Table A.1.

Table A.1 Coefficients of pressure correction equation and their values

Coefficient	Value
$a_{I+1,J}$	$(\rho dA)_{i+1,J}$
$a_{I-1,J}$	$(\rho dA)_{i,J}$
$a_{I,J+1}$	$(\rho dA)_{I,j+1}$
$a_{i,J-1}$	$(\rho dA)_{I,j}$
$b'_{I,J}$	$(\rho u^* A)_{i,J} - (\rho u^* A)_{i+1,J} + (\rho v^* A)_{I,j} - (\rho v^* A)_{I,j+1}$

The source term b' is the mass imbalance which arising from the incorrect velocity field u^* and v^*. By solving equation (A-15), the correction pressure (p') can be obtained at all points. Then, the correct pressure and correct velocities can be obtained by solving equations (A-5a) and (A-10)-(A-13), respectively.

The earlier approximation does not affect the final solution because the correction pressure and correction velocities will be zero in converged solution giving

$$p^* = p \text{ , } u^* = u \text{ and } v^* = v$$

The pressure correction is susceptible to divergence unless some under-relaxation is used during the iterative process and new, improved, pressure p^{new} are obtained with

$$p^{new} = p^* + \alpha_p p' \qquad \text{(A-16)}$$

where α_p is the pressure under-relaxation factor.

A correct choice of under-relaxation factor (α) is essential for cost-effective simulations. Too large value of α may lead to divergent iterative solutions and a

value which is too small will cause extremely slow convergence. Unfortunately, the values of under-relaxation factors are flow dependent and must be sought on a case-by-case basis. The procedure of SIMPLE algorithm is shown in Figure A.1.

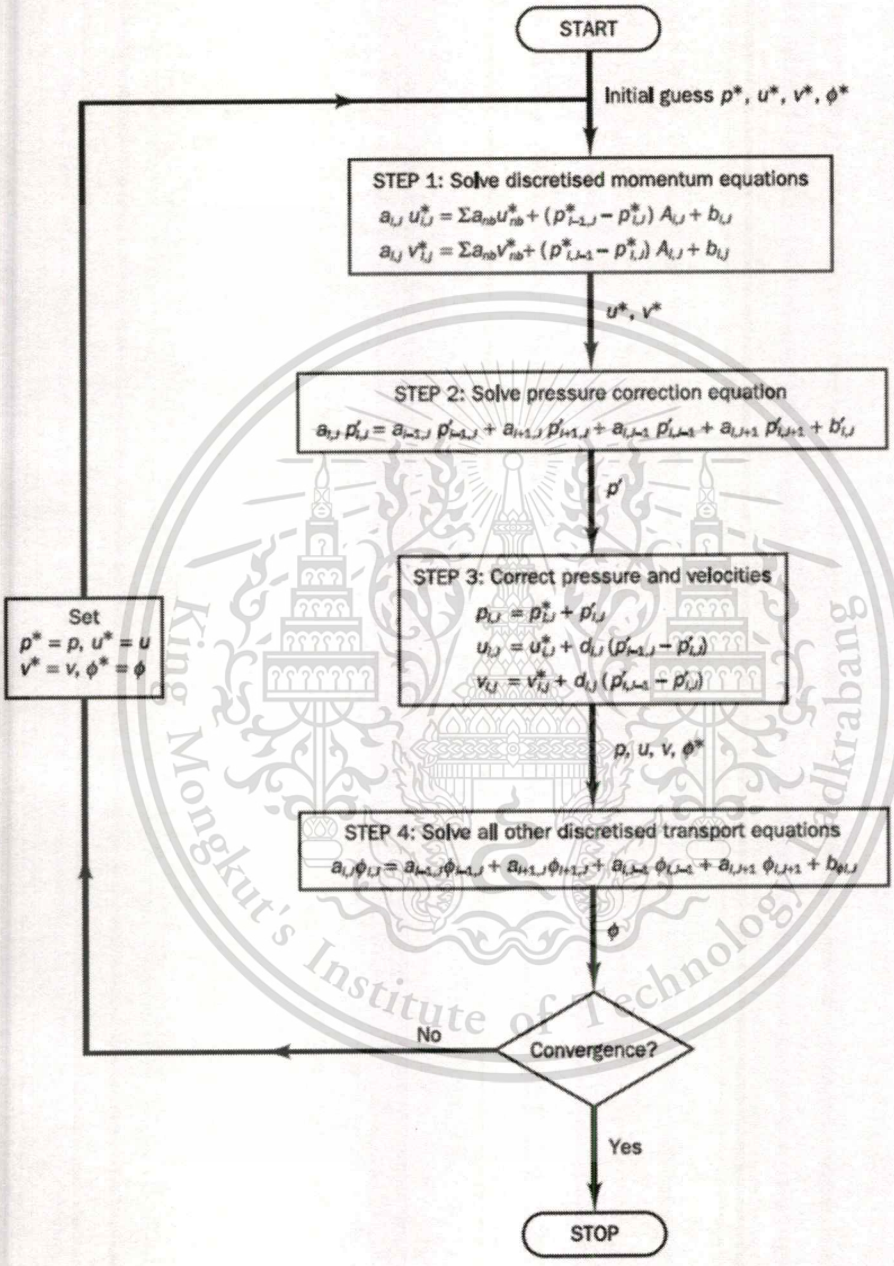

Figure A.1 The SIMPLE algorithm

APPENDIX B

CREATING AND MESHING MODEL BY USING GAMBIT

1. Start GAMBIT.

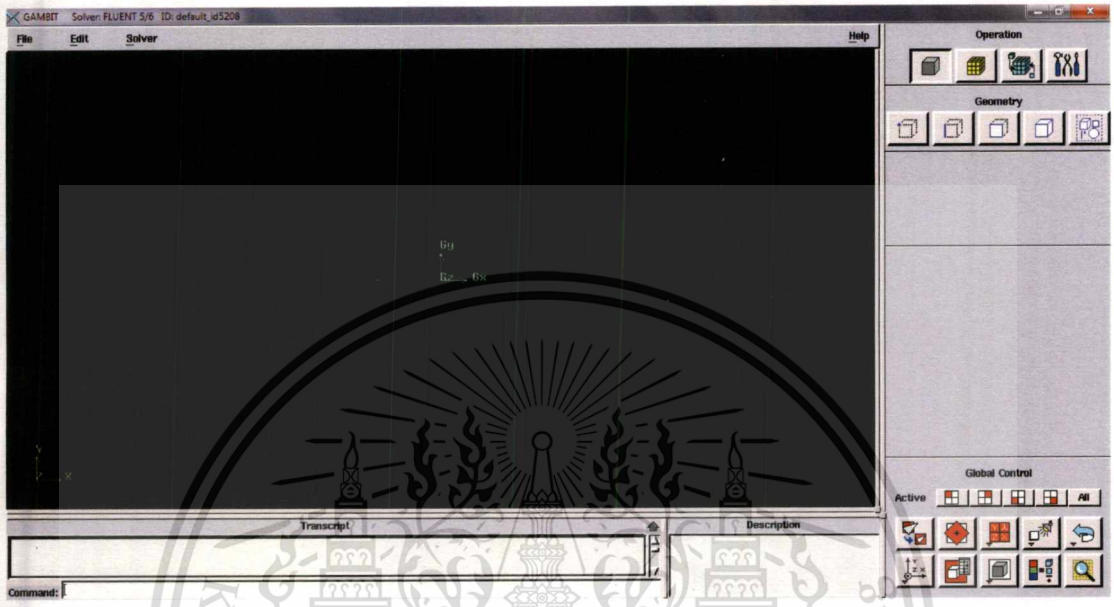

Figure B.1 The GAMBIT graphical user interface (GUI)

2. Create the coordinates (0,0), (0,0.0034), (0.0544,0), (0.0544,0.0034), (0,0.00001) and (0.0544,0.00001).

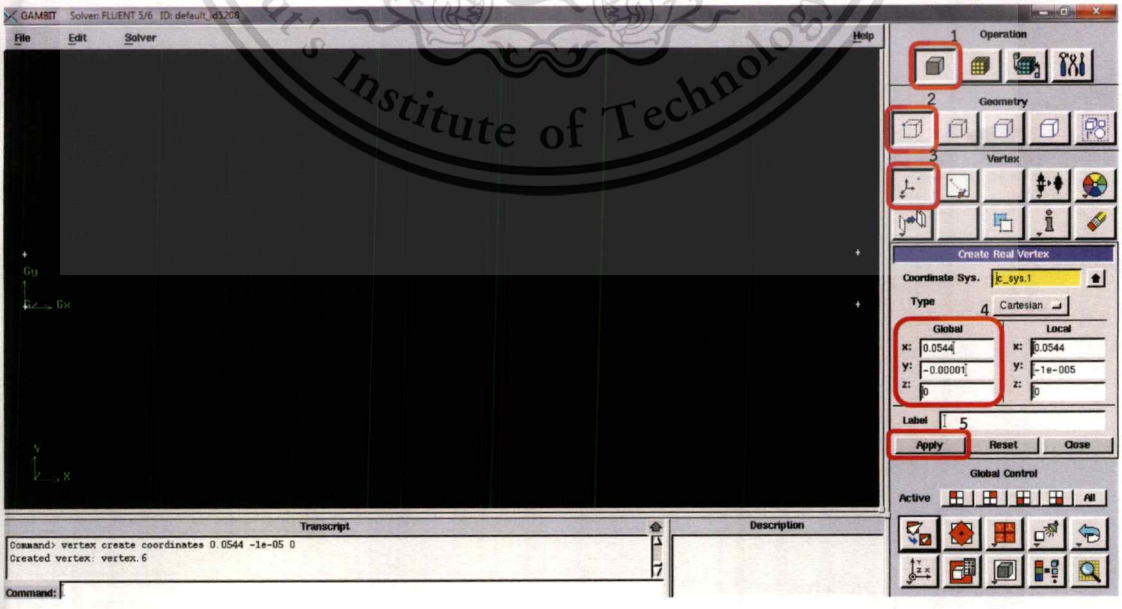

Figure B.2 Creating the coordinates

3. Create the lines.

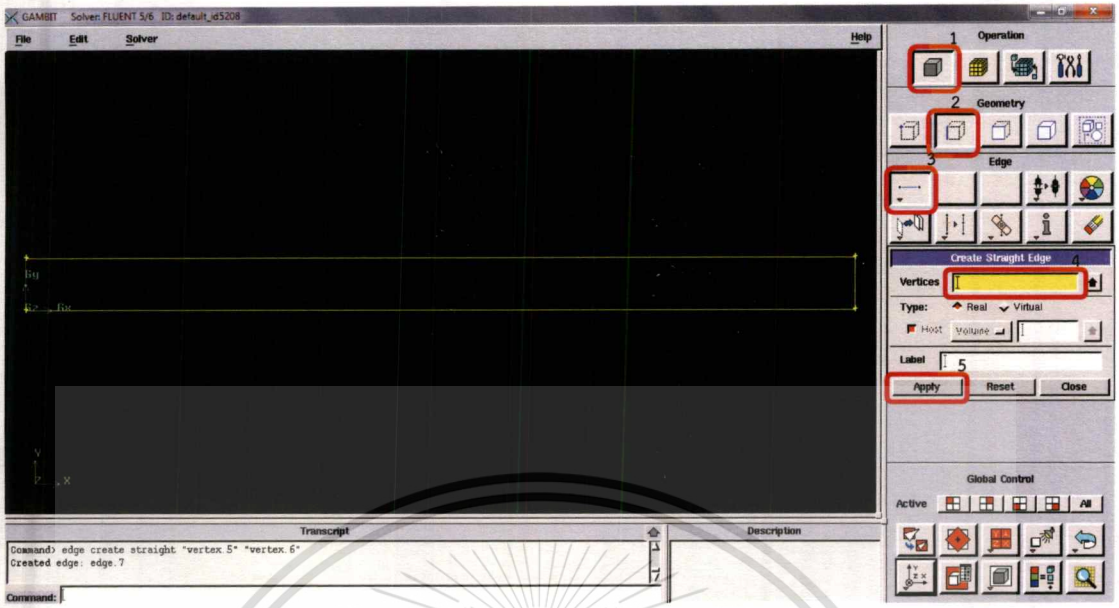

Figure B.3 Creating the lines

4. Create the coordinates (0.02916,0.0017), (0.03,0.0017), (0.03,0.00254) for 1st cylinder promoter and (0.04356,0.0017), (0.0444,0.0017), (0.0444,0.00254) for 2nd cylinder promoter.

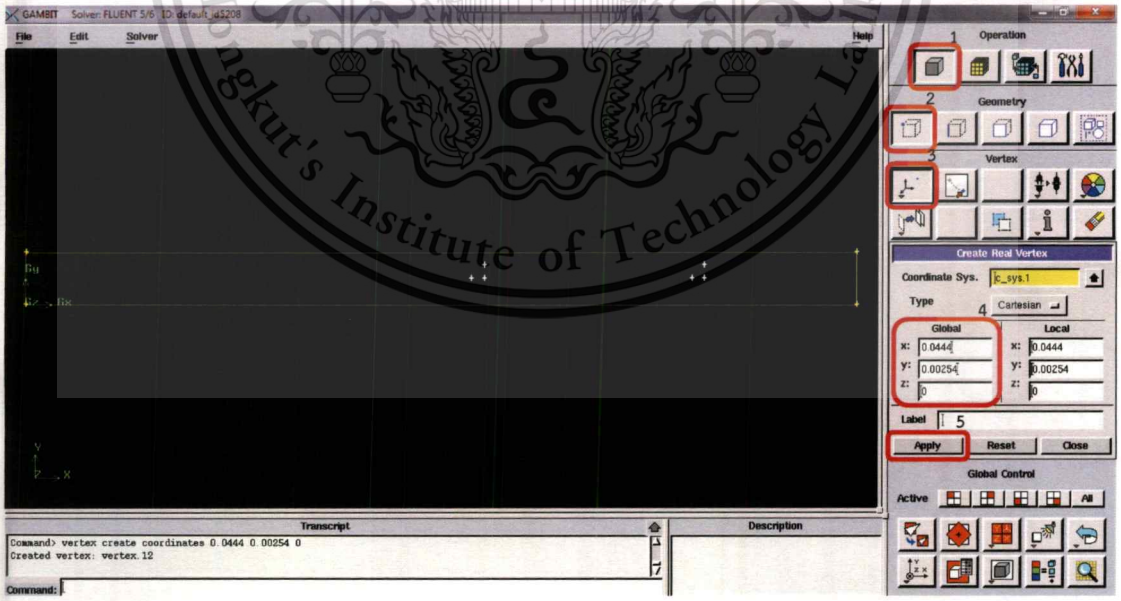

Figure B.4 Creating the coordinates for cylinder promoter

5. Create the cylinders.

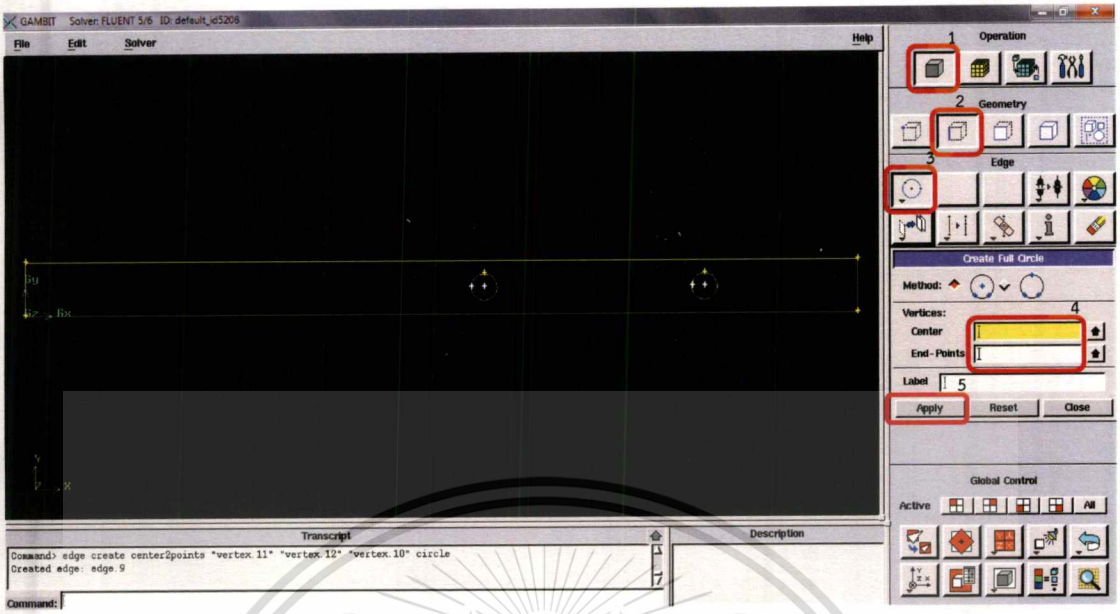

Figure B.5 Creating the cylinders

6. Create the faces including face 1 (above membrane), face 2 (under membrane), face 3 (1st cylinder) and face 4 (2nd cylinder).

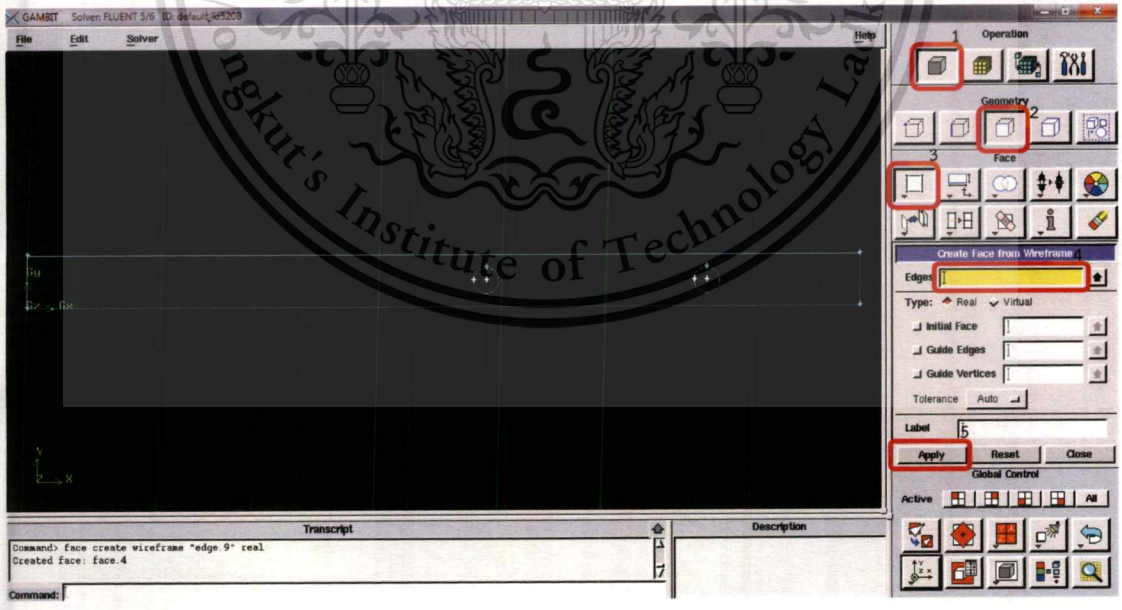

Figure B.6 Creating the faces

7. Spit rectangular domain (face 1) with cylinder promoters (face 3 and 4).

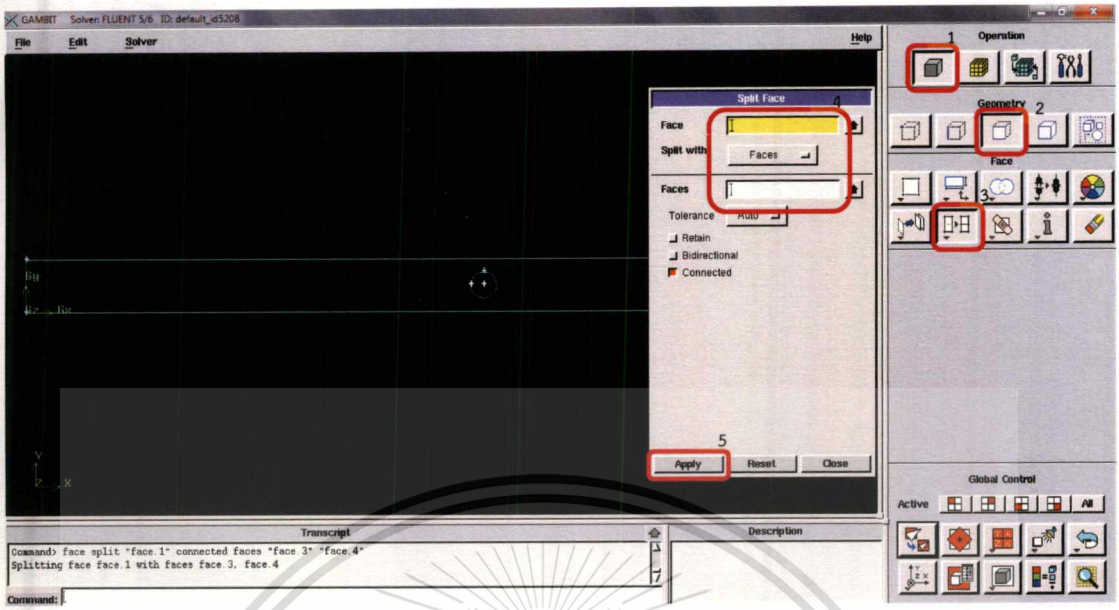

Figure B.7 Spiting face

8. Create the boundary layer at membrane line (y=0).

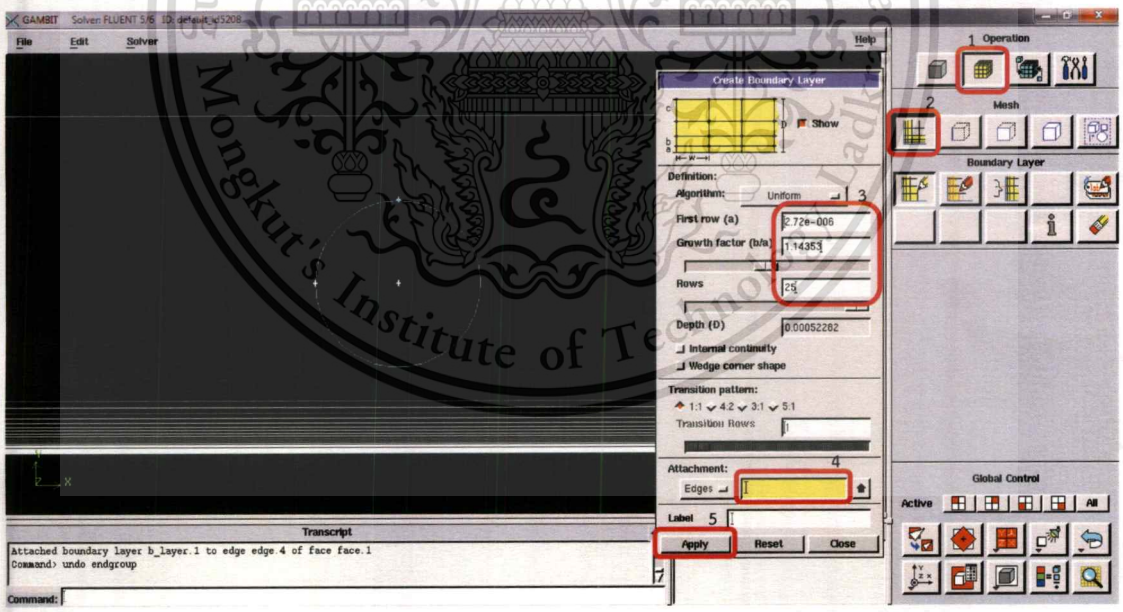

Figure B.8 Boundary layer at membrane

9. Create the mesh of face 1.

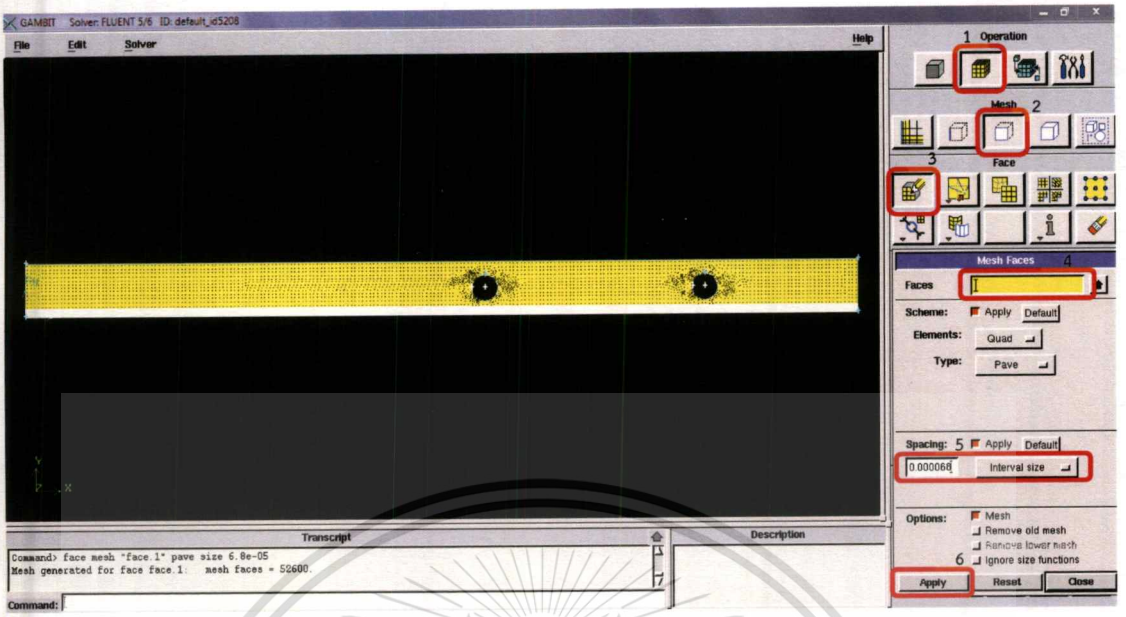

Figure B.9 Meshing face 1

10. Create the mesh edges at the side of face 2.

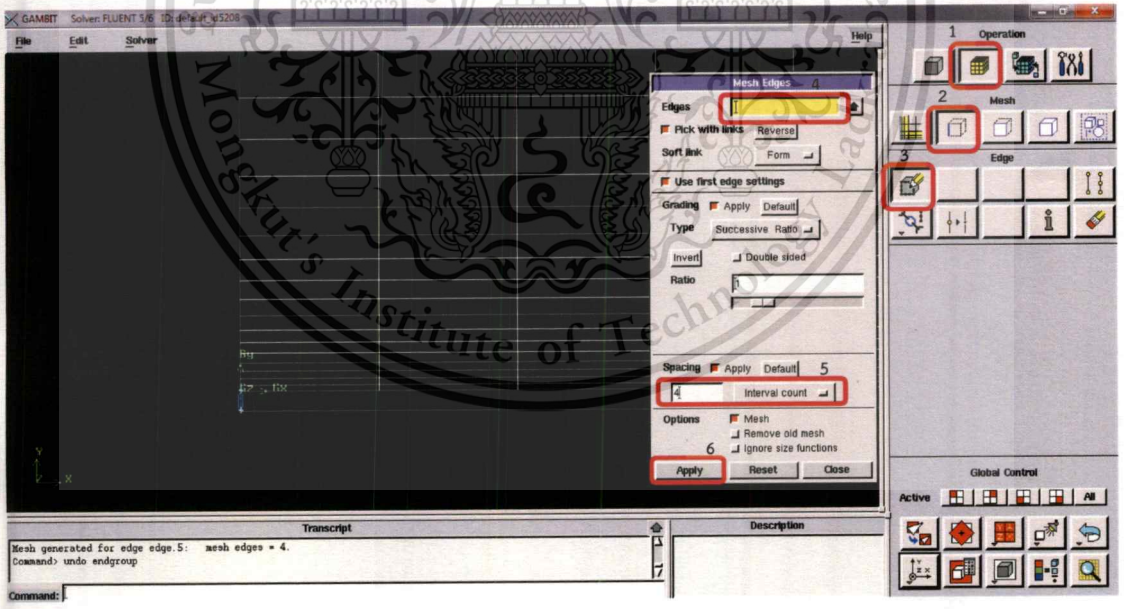

Figure B.10 Meshing edges

11. Create the mesh of face 2.

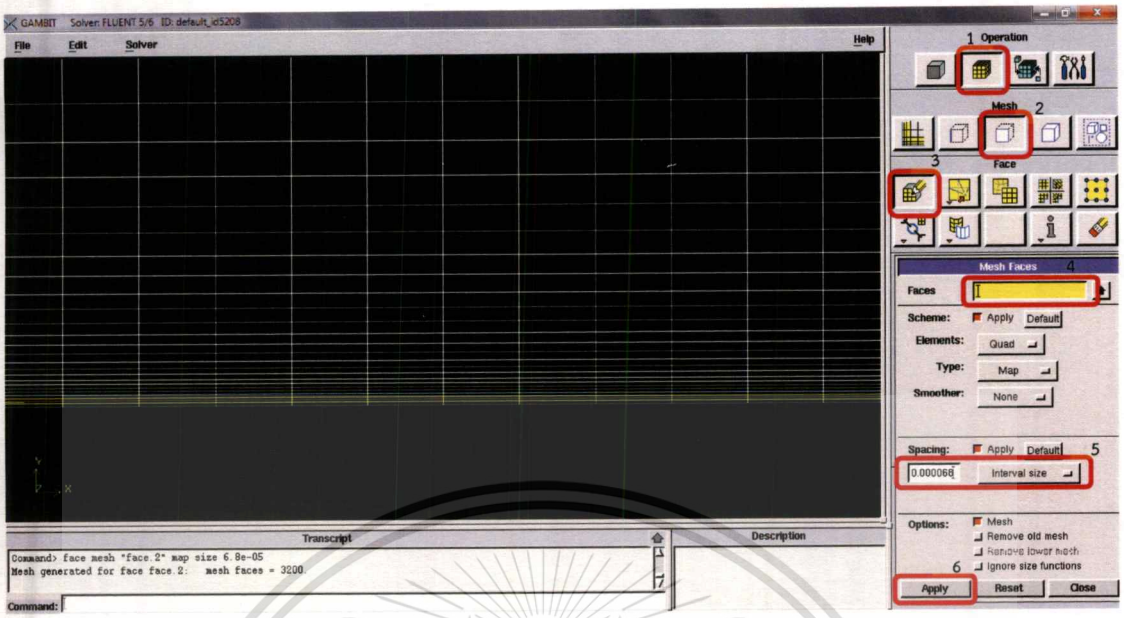

Figure B.11 Meshing face 2

12. Specify boundary Types.

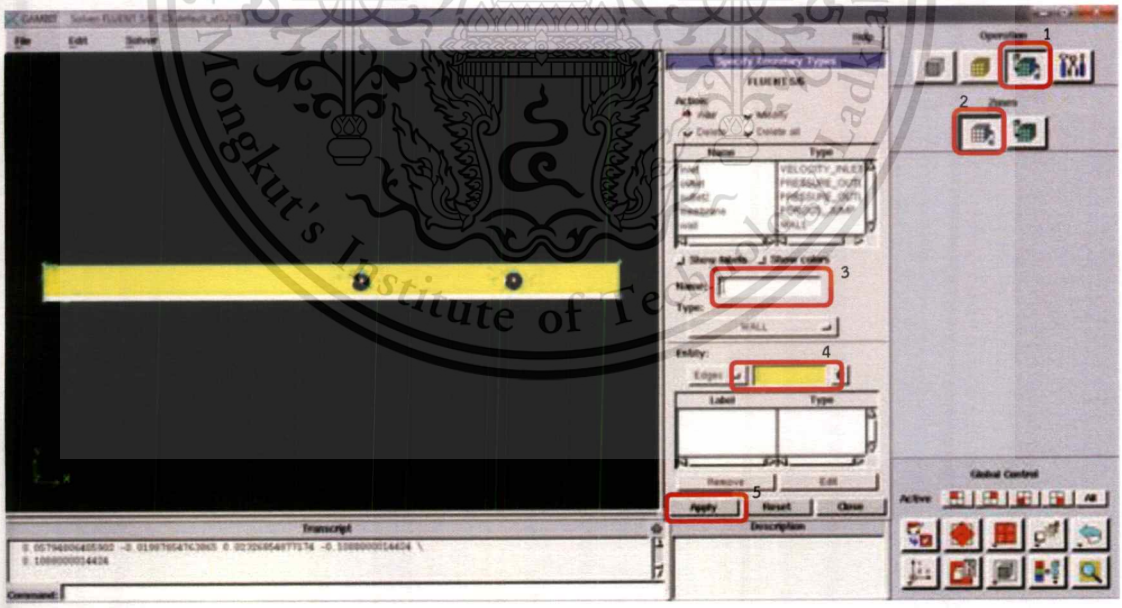

Figure B.12 Specify boundary Types

13. Specify continuum Types.

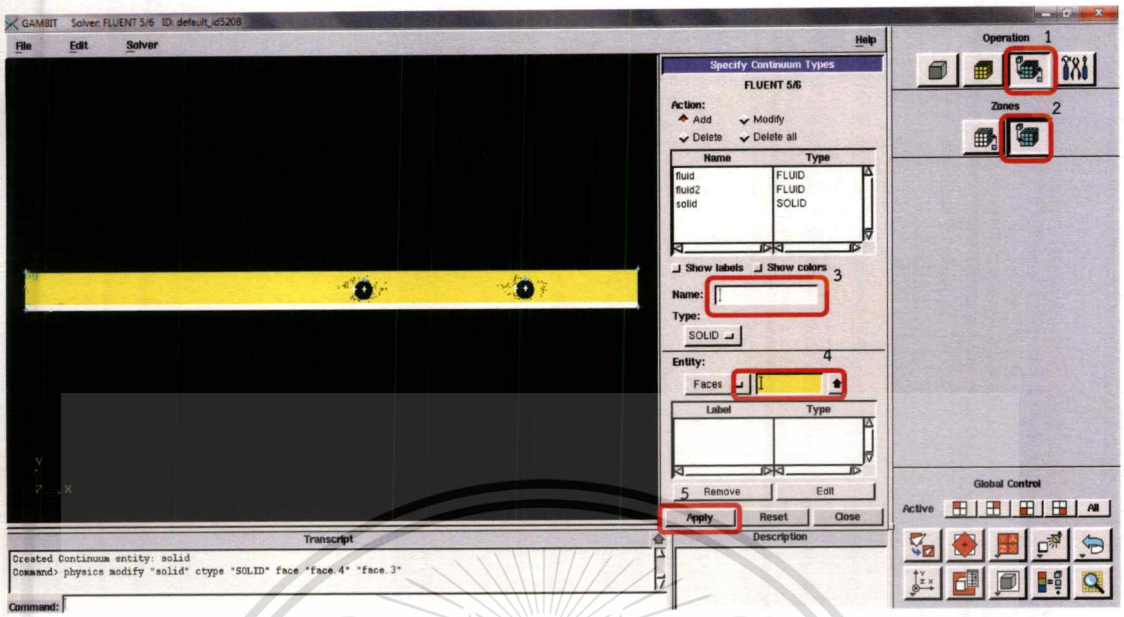

Figure B.13 Specify continuum Types

14. Save as the model as Cylinder promoter.

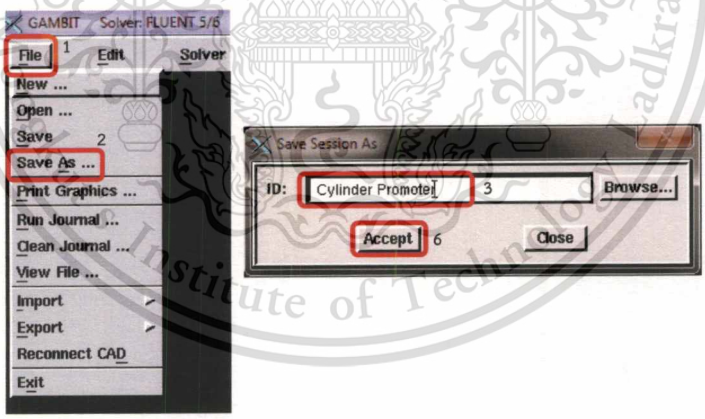

Figure B.14 Save the model

15. Export mesh to FLUENT.

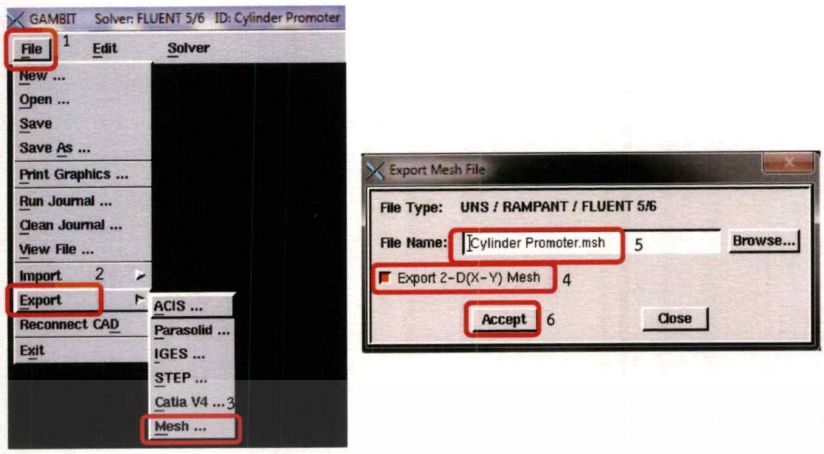

Figure B.15 Export mesh

Remark: The creation and grid generation of the others turbulence promoters are similar to the previous step.

APPENDIX C
SOLUTION BY USING FLUEN

1. Start FLUENT.

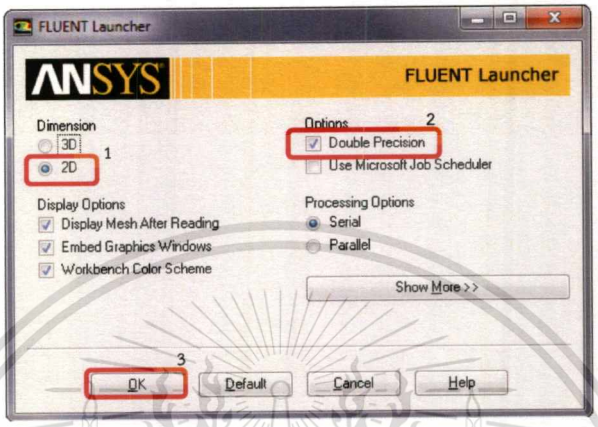

Figure C.1 Window of FLUENT

2. Read the mesh file (cylinder promoter.msh).

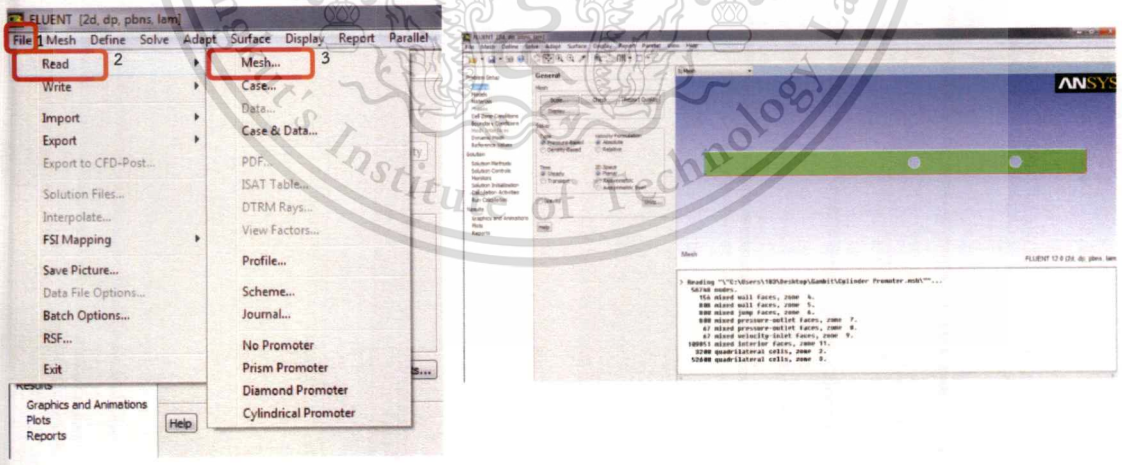

Figure C.2 Reading the mesh

3. Enable the gravity and set the value.

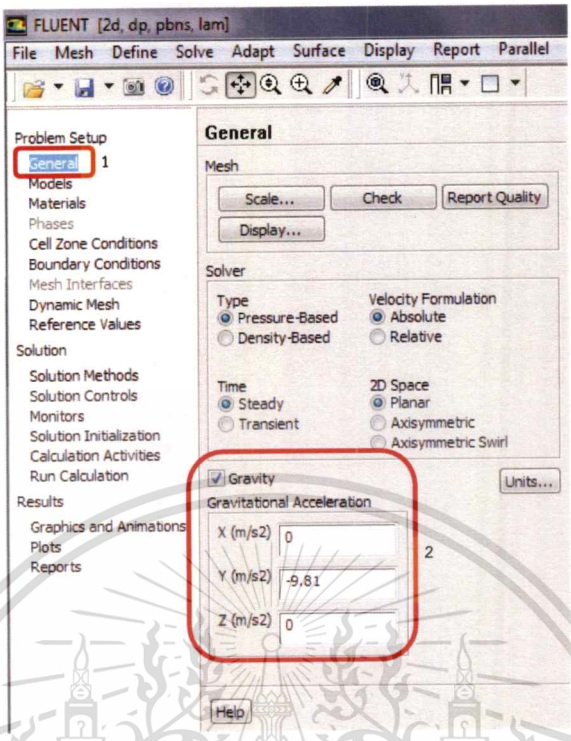

Figure C.3 Setting the gravity

4. Scale the mesh.

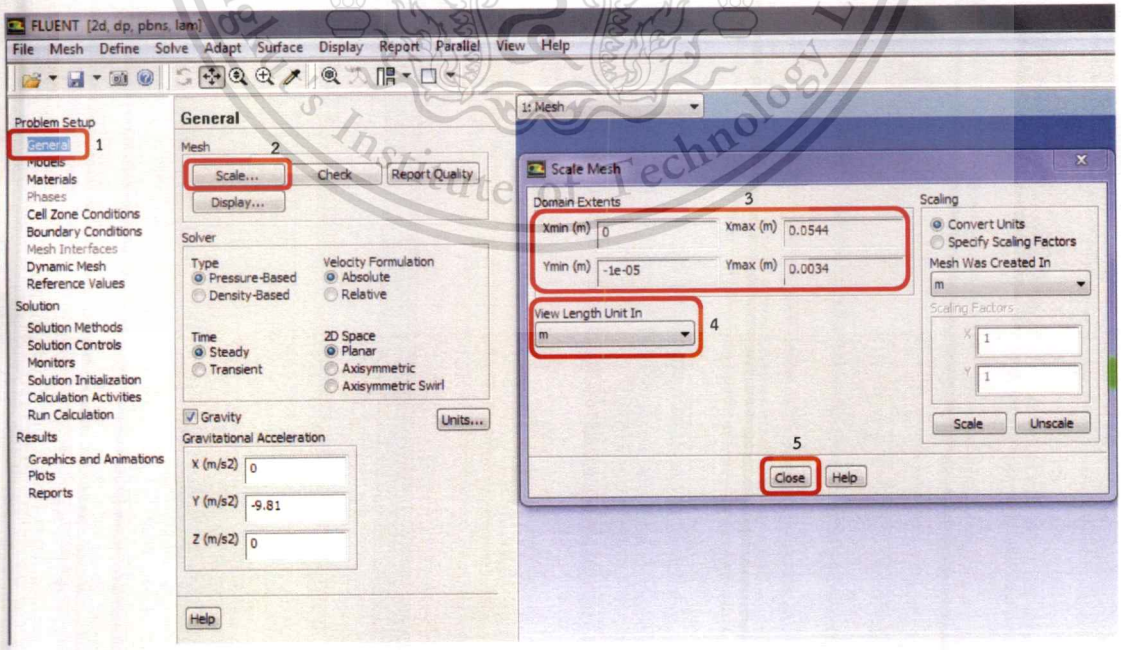

Figure C.4 Setting the scale mesh

5. Check the mesh.

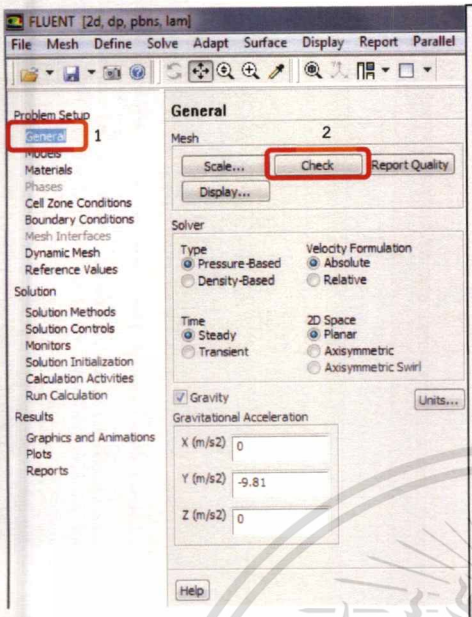


```
Mesh Check

Domain Extents:
  x-coordinate: min (m) = 0.000000e+000, max (m) = 5.440000e-002
  y-coordinate: min (m) = -1.000000e-005, max (m) = 3.400000e-003
Volume statistics:
  minimum volume (m3): 1.466250e-010
  maximum volume (m3): 9.216073e-009
   total volume (m3): 1.810754e-004
Face area statistics:
  minimum face area (m2): 2.150000e-006
  maximum face area (m2): 1.594295e-004
Checking number of nodes per cell.
Checking number of faces per cell.
Checking thread pointers.
Checking number of cells per face.
Checking face cells.
Checking cell connectivity.
Checking bridge faces.
Checking right-handed cells.
Checking face handedness.
Checking face node order.
Checking element type consistency.
Checking boundary types:
Checking face pairs.
Checking periodic boundaries.
Checking node count.
Checking nosolve cell count.
Checking nosolve face count.
Checking face children.
Checking cell children.
Checking storage.
Done.
```

Figure C.5 Mesh check

6. Set fluid flow equation.

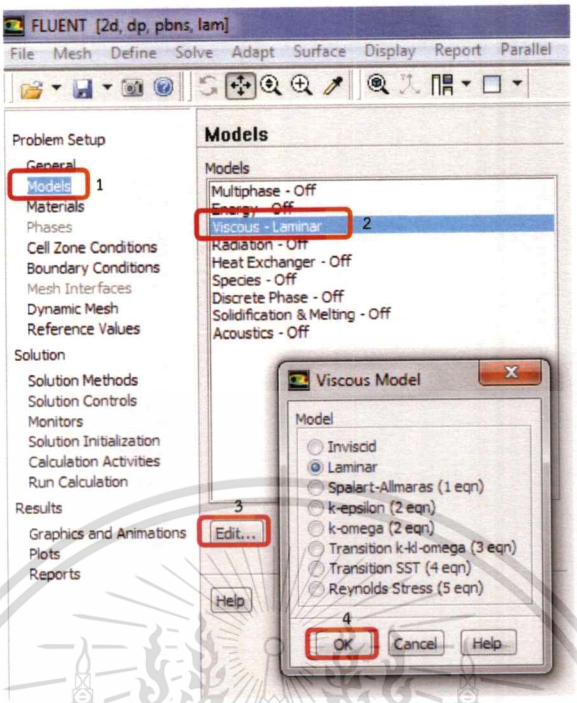

Figure C.6 Setting the model

7. Create a new fluid (fruit juice).

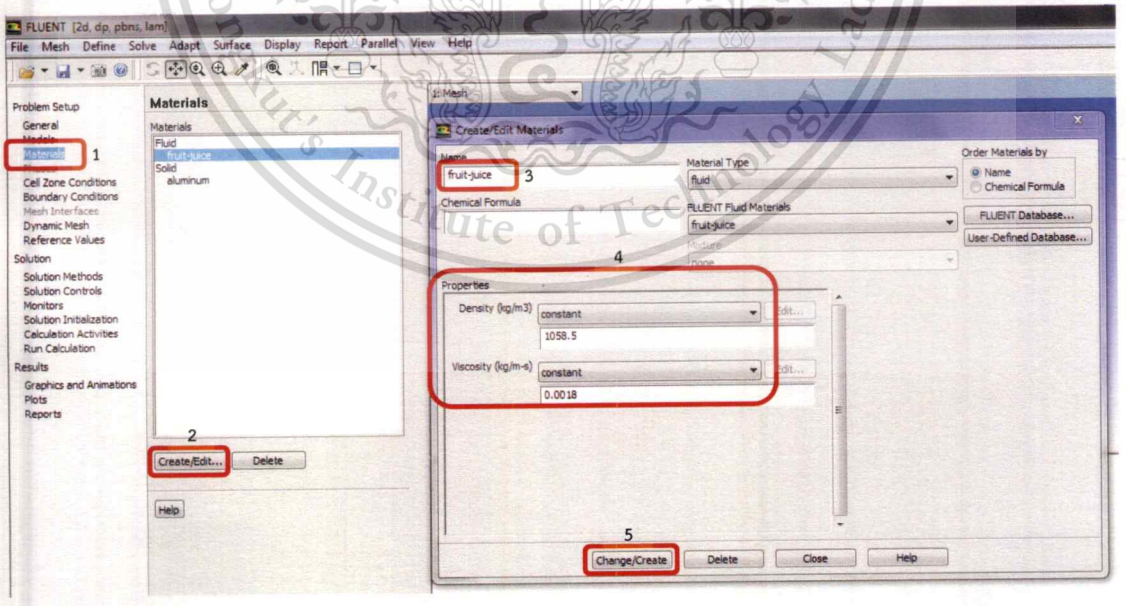

Figure C.7 Setting the material

8. Set the cell zone conditions for the fluid zone.

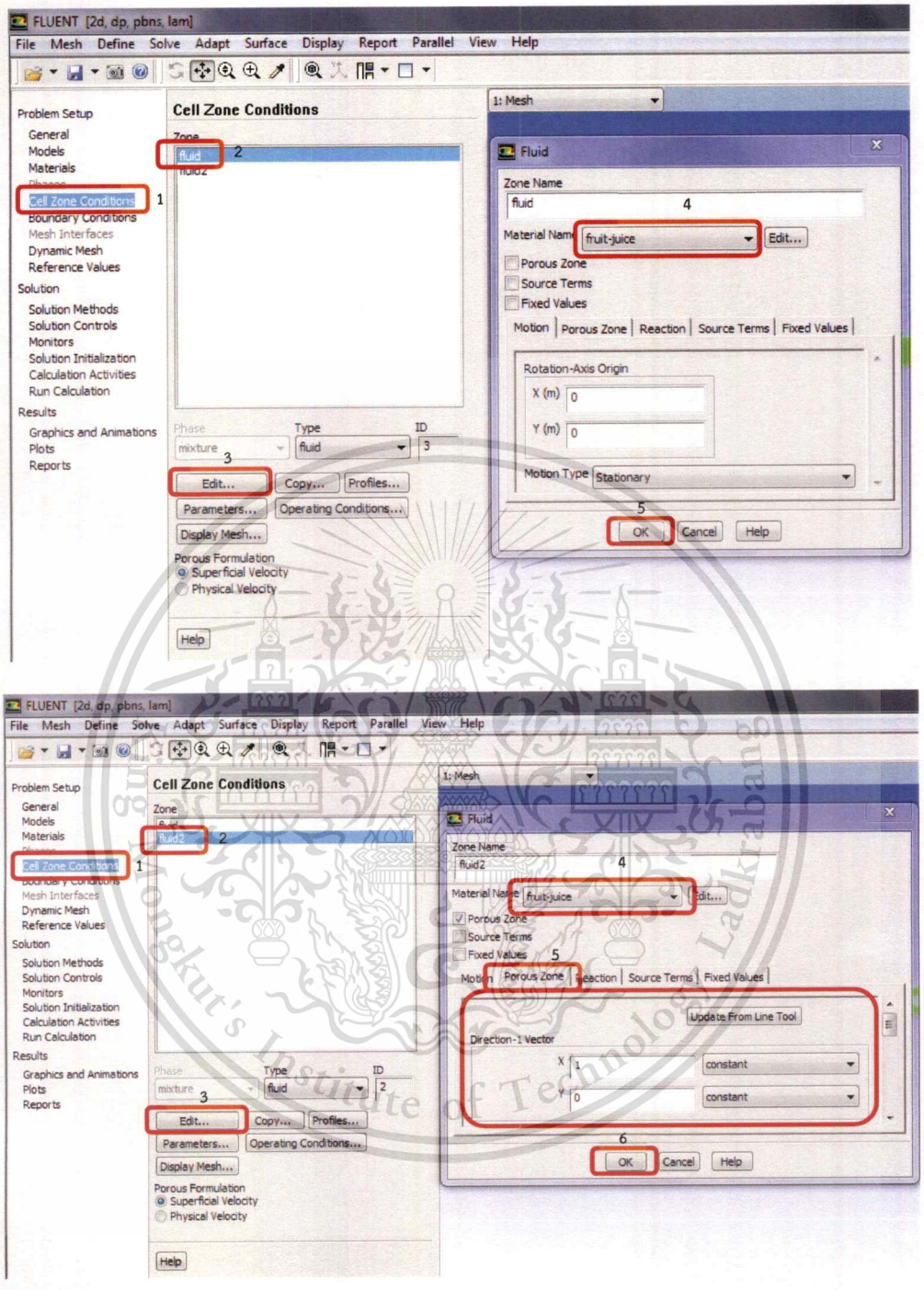

Figure C.8 Setting the cell zone conditions

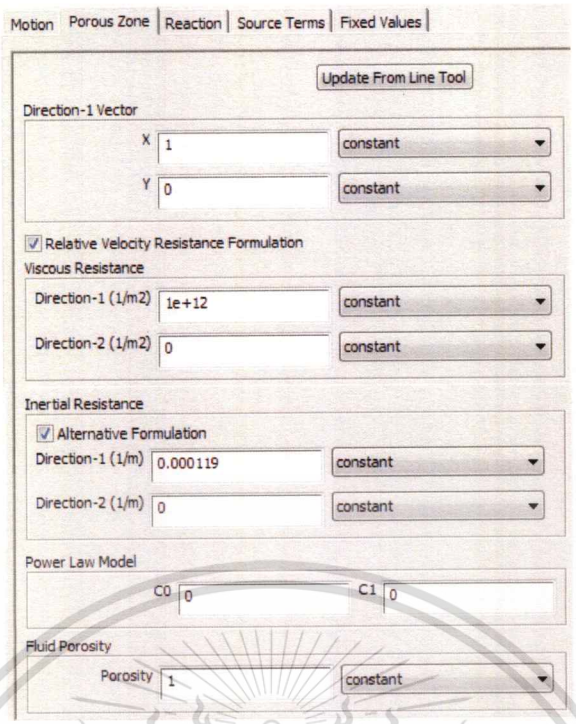

Figure C.9 Setting porous zone

9. Set the boundary conditions for inlet, membrane, outlet and outlet2, respectively.

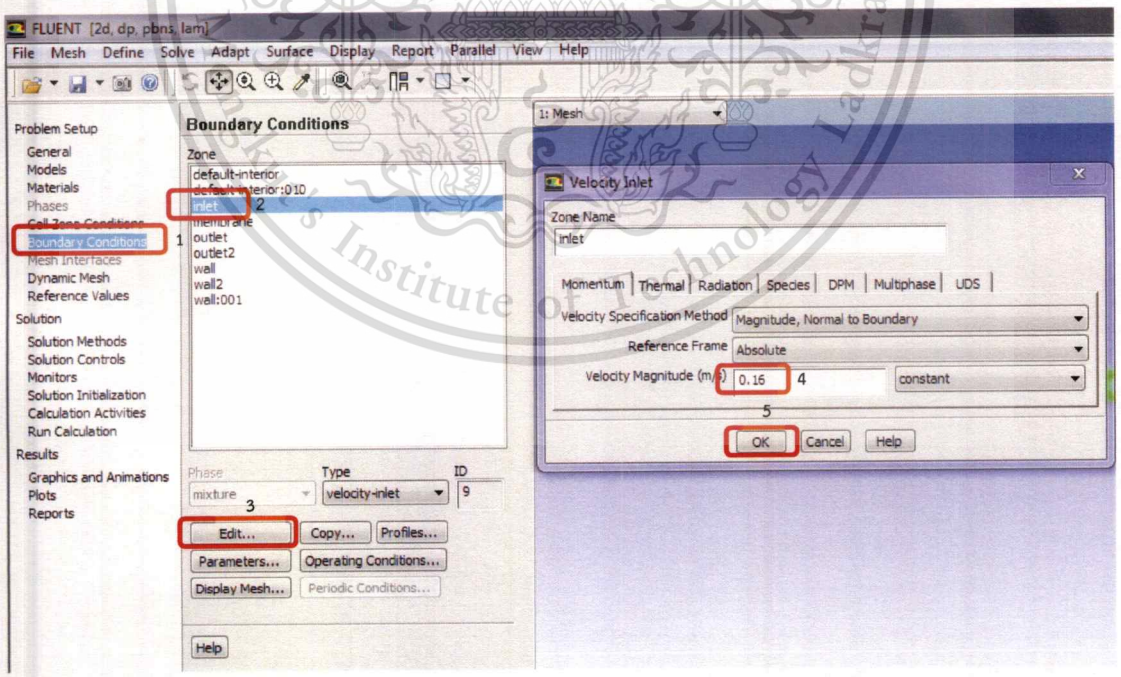

Figure C.10 Setting boundary conditions at inlet

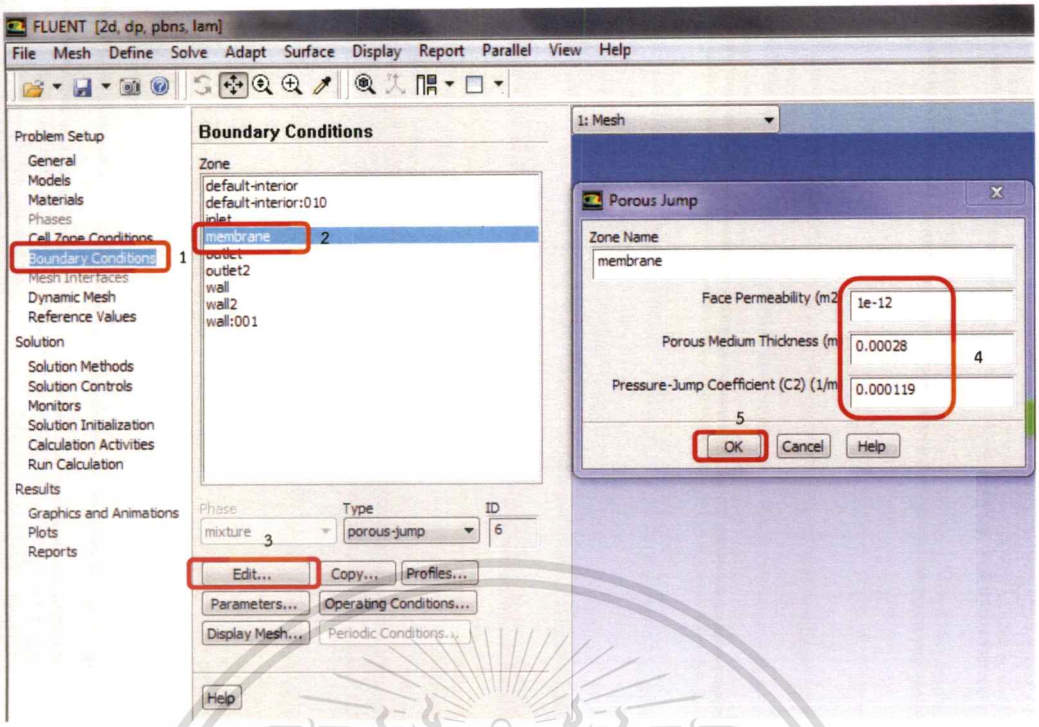

Figure C.11 Setting boundary conditions at membrane

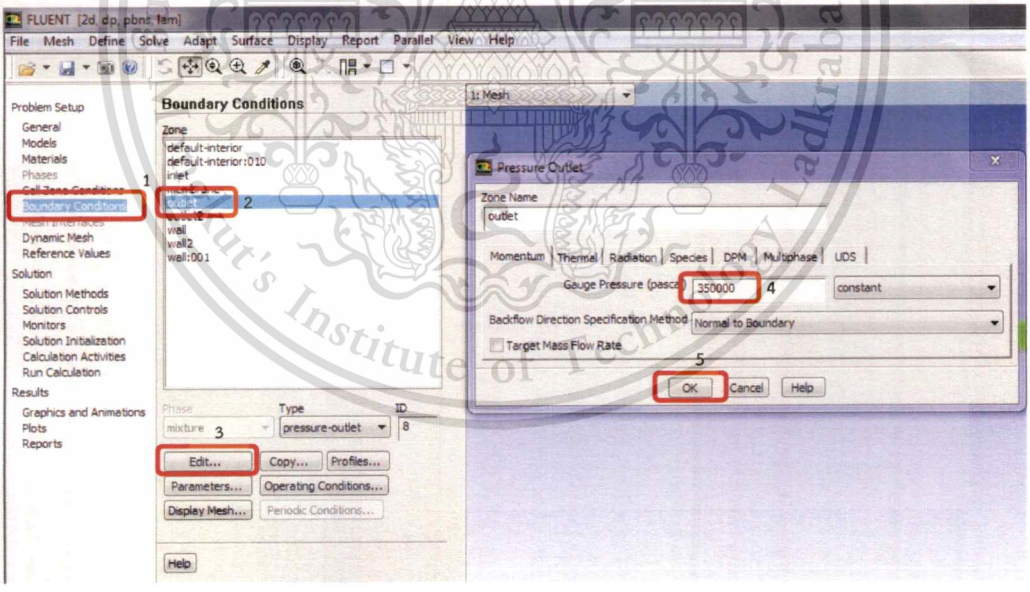

Figure C.12 Setting boundary conditions at outlet

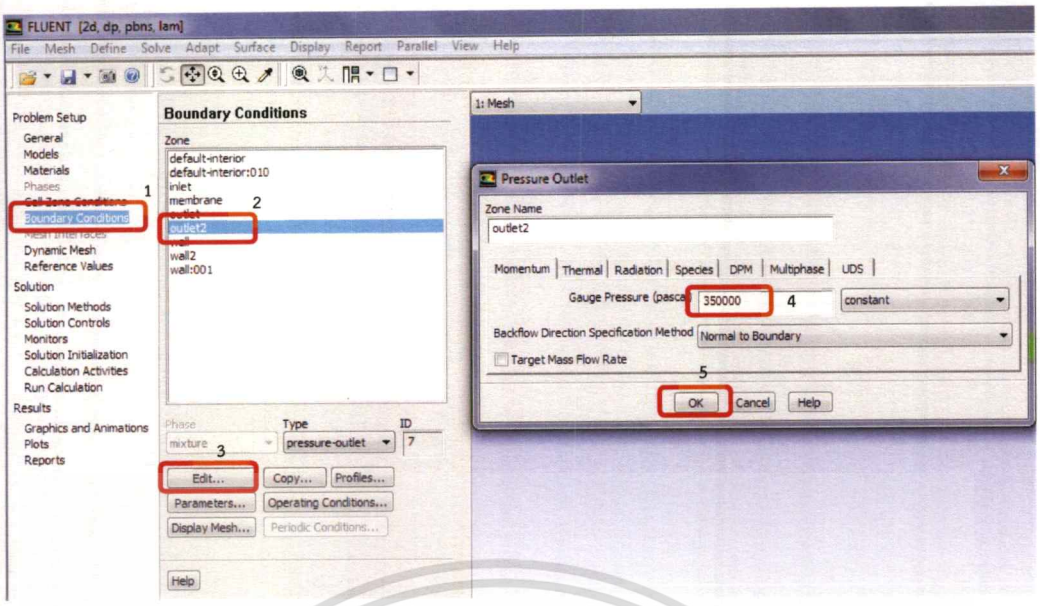

Figure C.13 Setting boundary conditions at outlet2

10. Set the solution method.

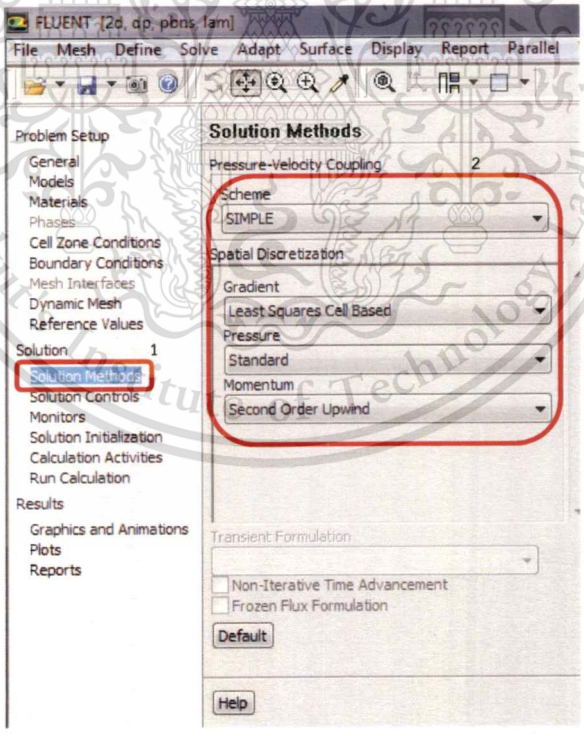

Figure C.14 Setting boundary solution methods

11. Set the residual monitors.

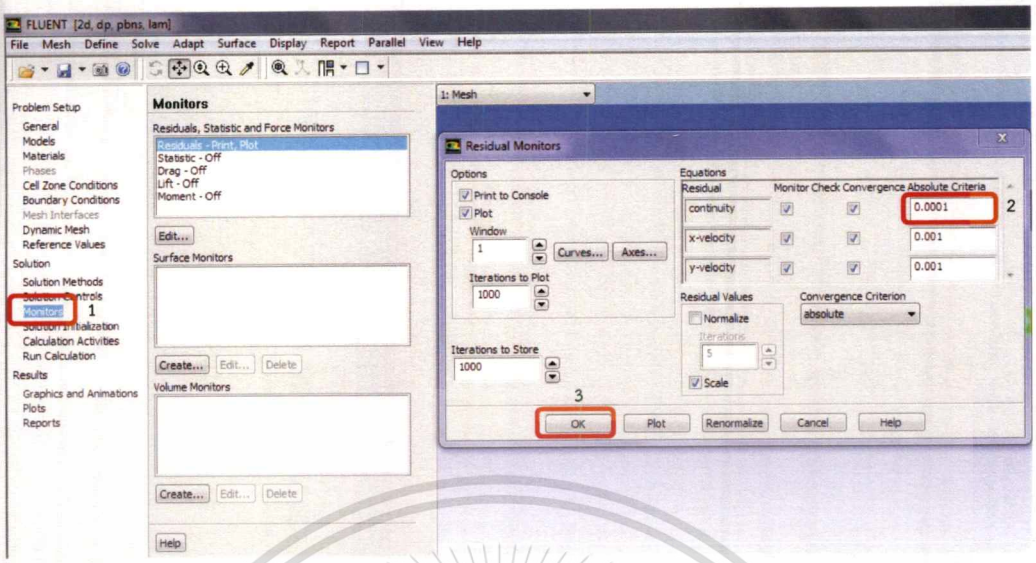

Figure C.15 Setting Monitors

12. Initialize the solution.

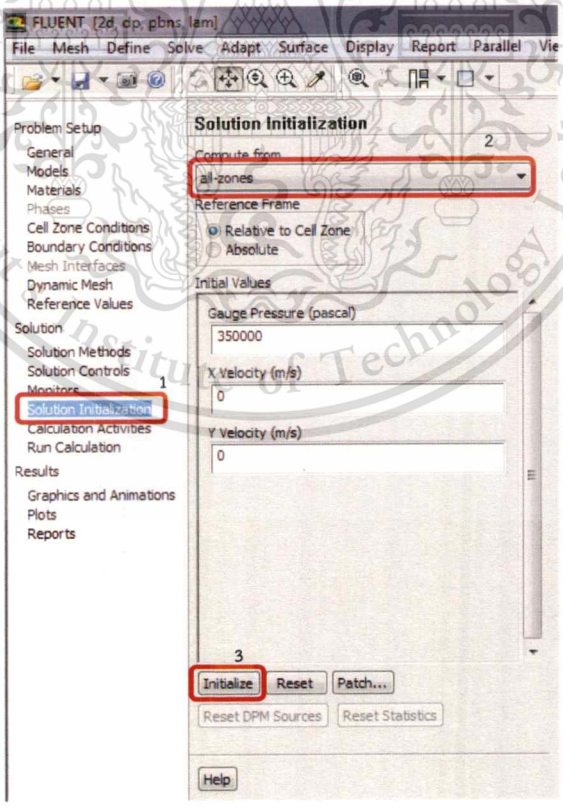

Figure C.16 Setting solution initialization

13. Start the calculation.

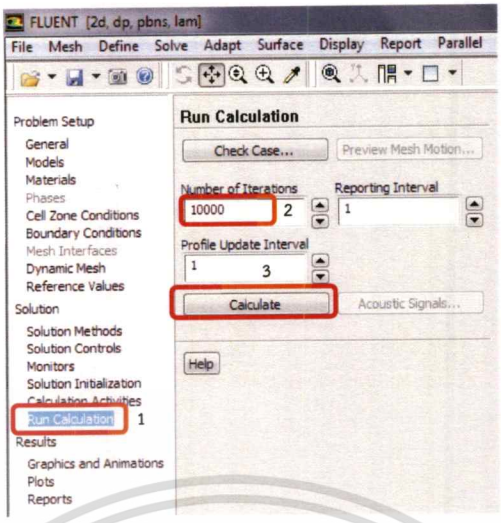

Figure C.17 Setting run calculation

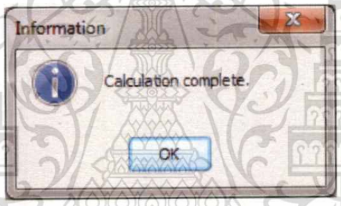

Figure C.18 Window of calculation complete

15. Save the case and data files.

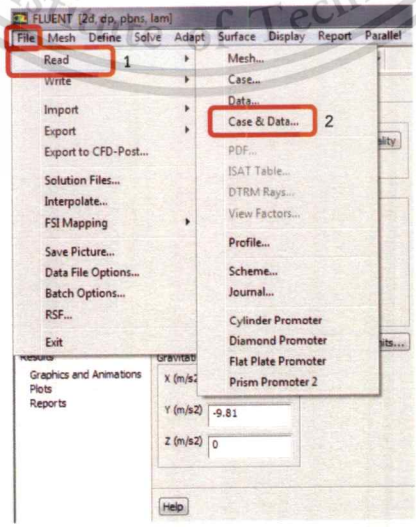

Figure C.19 Save the files

16. Set the contour of x-velocity.

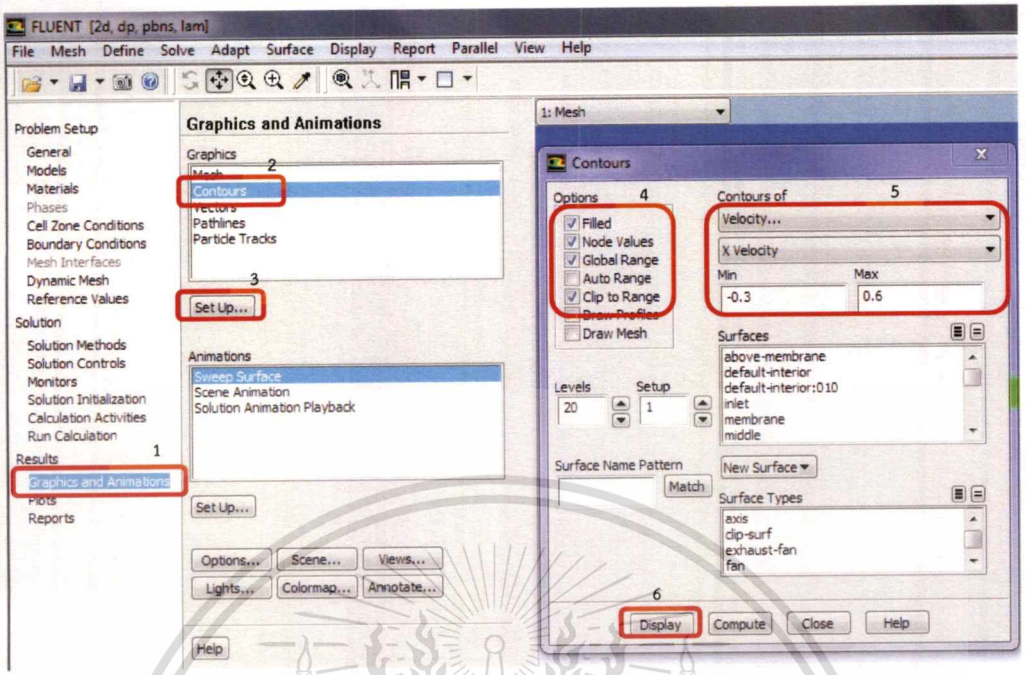

Figure C.20 Setting of x-velocity contour

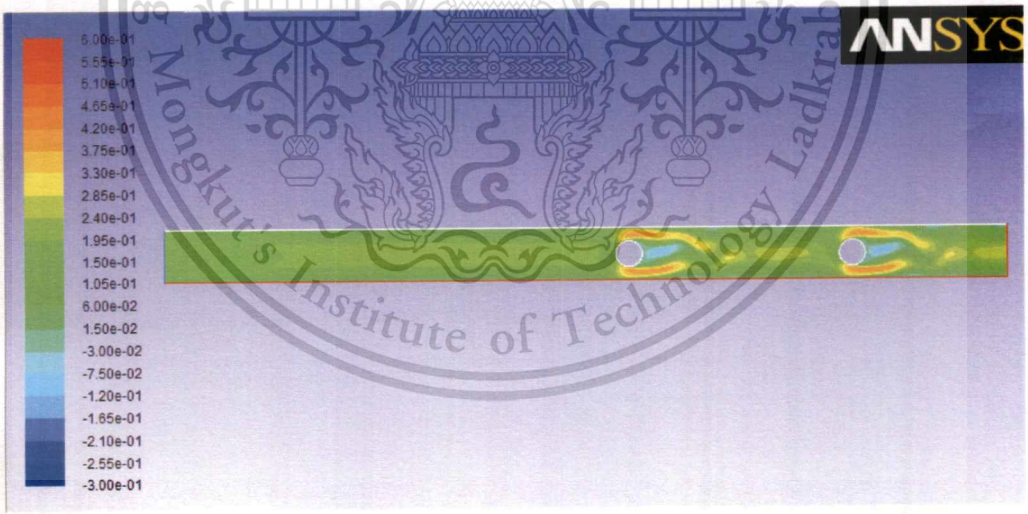

Figure C.21 Contour of x-velocity

17. The calculation of the permeate flux.

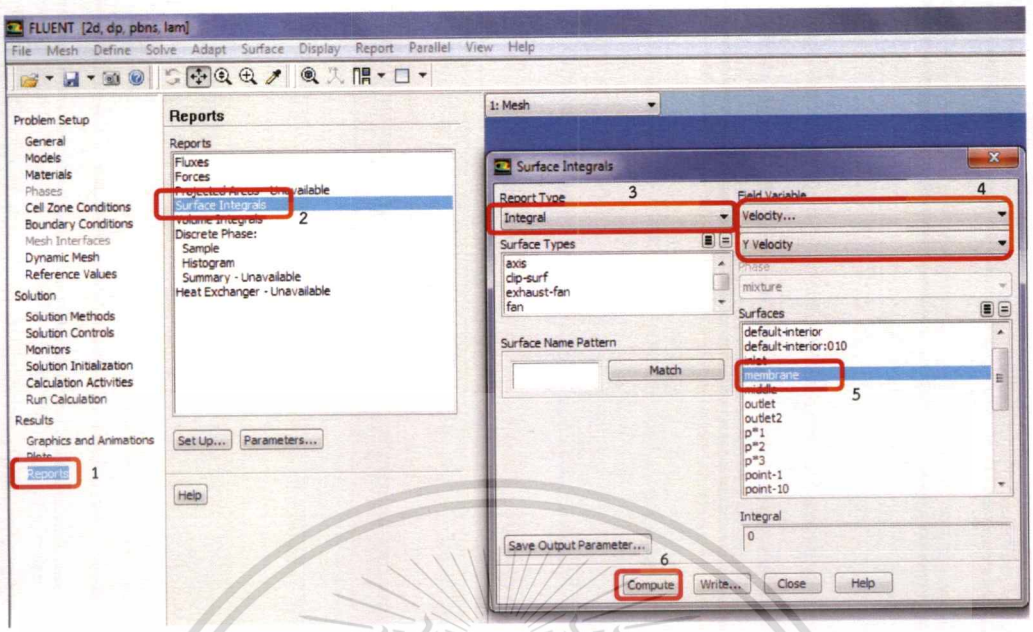

Figure C.22 Setting for calculation the permeate flux

18. Create the line underneath turbulence promoter.

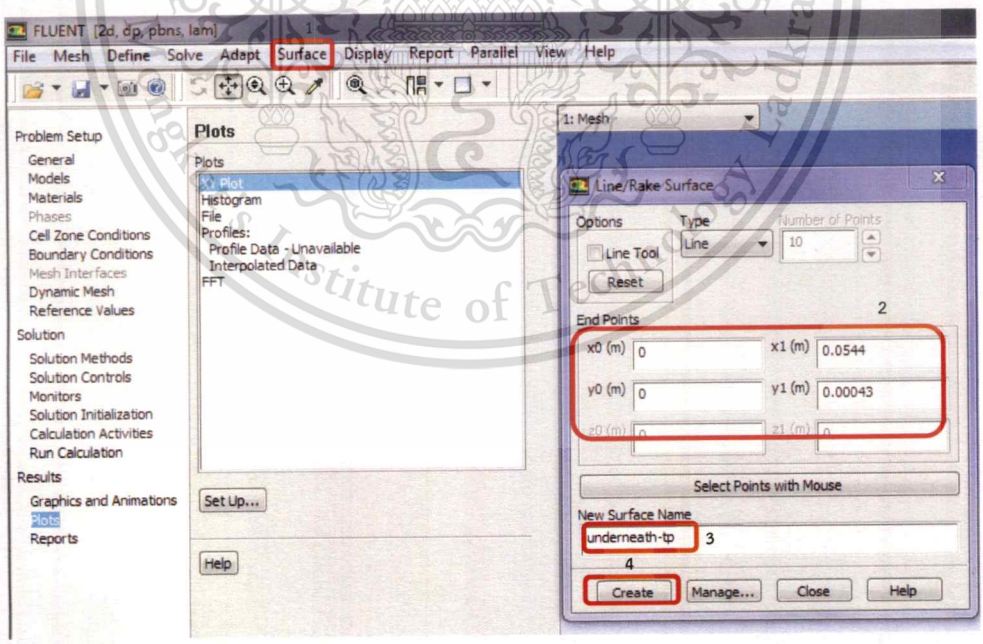

Figure C.23 Creating the line

19. Write the data of y-velocity underneath turbulence promoter.

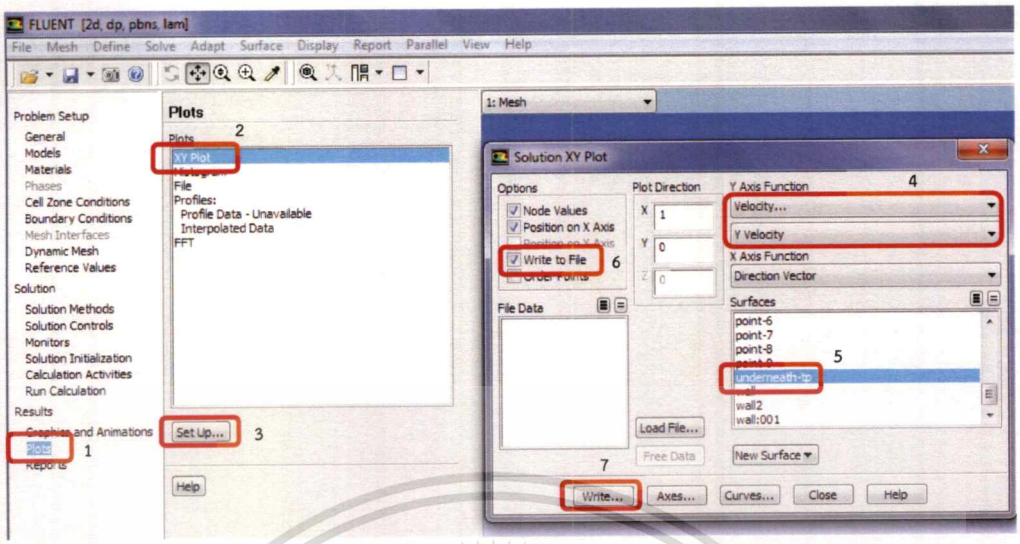

Figure C.24 Writing the data of y-velocity

20. Create the points lower surface of turbulence promoter.

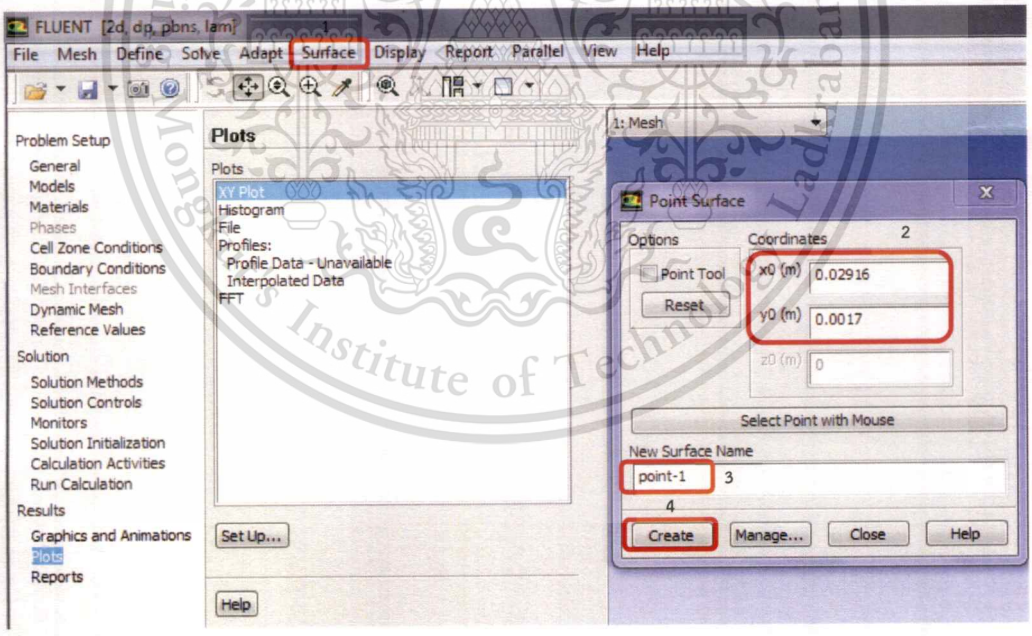

Figure C.25 Creating the point

21. Write the data of x-velocity lower surface of turbulence promoter.

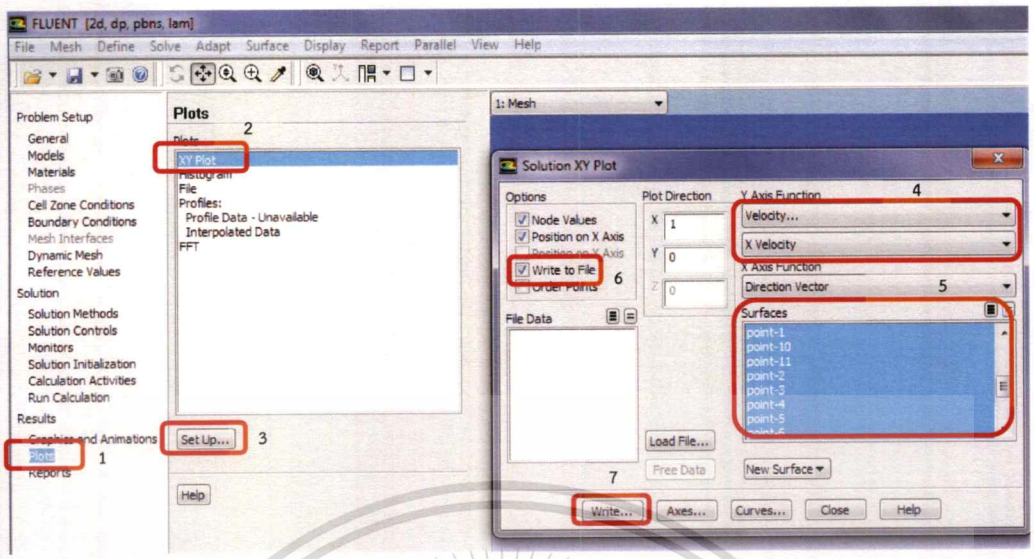

Figure C.26 Writing the data of x-velocity

22. The calculation of the static pressure.

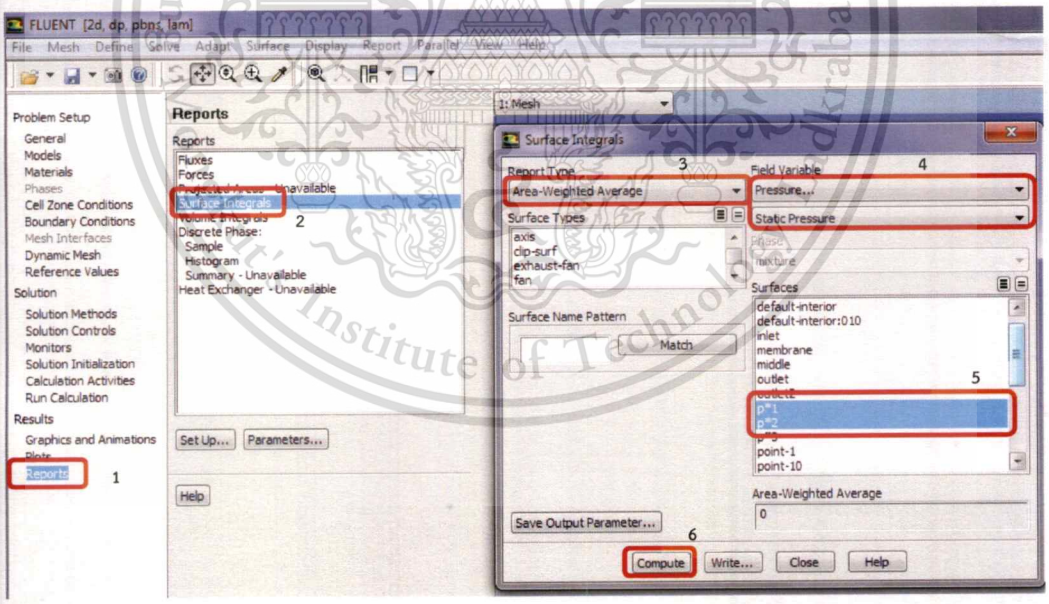

Figure C.27 Setting for calculation the static pressure

Remark: The solutions by using FLUENT of the others turbulence promoters are similar to the previous step.

APPENDIX D
LIST OF PUBLICATION

Wanthamanee S., Bumrungthaichaichan E., Wattananusorn S. "Influence of Turbulence promoter Geometry on Flow Pattern in Cross-Flow Membrane Ultrafiltration." **Ladkrabang Engineering Journal**, vol. 29, 2012. pp. 48-53

VITA

NAME	Miss Supawadee Wanthamanee
DATE OF BIRTH	October 2, 1985
EDUCATIONAL RECORD	
HIGH SCHOOL	High School Graduation Ratwinit Bangkaeo School, 2004
BACHELOR'S DEGREE	Bachelor of Engineering (Food Engineering) King Mongkut's Institute of Technology Ladkrabang, 2008
MASTER'S DEGREE	Master of Engineering (Chemical Engineering) King Mongkut's Institute of Technology Ladkrabang, 2013

ISSN 0125-1724

วิศวสารลาดกระบัง

LADKRABANG ENGINEERING JOURNAL

Faculty of Engineering, King Mongkut's Institute of Technology Ladkrabang

คณะวิศวกรรมศาสตร์ สถาบันเทคโนโลยีพระจอมเกล้าเจ้าคุณทหารลาดกระบัง

Volume 29 Number 2 June 2012

Academic Papers

Research Papers

Influence of Turbulence Promoter Geometry on Flow Pattern in Cross-Flow Membrane Ultrafiltration

Supawadee Wanthamanee Eakarach Bumrungthaichaichan Santi Wattananusorn
Department of Chemical Engineering, Faculty of Engineering, King Mongkut's Institute of Technology Ladkrabang

Abstract

In this work, the effects of turbulence promoter geometry on flow pattern were studied. The commercial CFD package FLUENT, which employs the finite-volume method, was used for numerical computations. The simulation models were performed in cross-flow membrane using three types of turbulence promoters. The results show that the presence of turbulence promoters causes remarkable increases of the fluid velocity and generate the region of unsteady flow, which can significantly improve the filtration performance. The flux enhancement is also attributed to the intense fluctuations, which can greatly disrupt the development of boundary layer, as well as the growth of cake layer. Among the three types of turbulence promoters, the prism shape showed better performances than the others did.

Keywords: CFD, turbulence promoter, membrane ultrafiltration

1. Introduction

Ultrafiltration (UF) is a membrane pressure driven process with numerous industrial applications in the purification and separation, such as chemical processing, wastewater handling, drug delivery medium etc., because of its high efficiency and low energy consumed.

However, its performance in many applications is limited by membrane fouling which causes decay in filtrate flux and high cost of membrane filtration process. This phenomenon refers to the deposit of rejected particles of the feed on the surface of the membrane leading to a cake layer building (external fouling) or to adsorption of small particles within the membrane pores (internal fouling). Therefore, in order to prevent this phenomenon a good understanding of the mechanism is necessary.

Various membrane fouling controlling techniques have been used to enhance membrane flux, such as the applying of additional electric fields and ultrasonic fields, the adoption of rotating membranes, membrane surface modification, rapid backflushing pulsing and shocking, feed pretreatment, gas sparging and other methods. Except those techniques, turbulence promoter can be more simple and effective in overcoming membrane fouling and enhancing membrane flux [1].

In recent year, analyses for the hydrodynamics and the fluid flow pattern adjacent the membrane have studied and visualized by computational fluid dynamics (CFD) mathematical modeling and simulation. Cao et al., [2] tested the effects of various arrangements of cylindrical turbulence promoters on fluid flow hydrodynamics. The detailed flow pattern, velocity distributions and turbulence kinetic energy distributions in a spacer filled channel are shown in their study. Significant flux enhancement was achieved using turbulence promoters in a position perpendicular to the flow direction for ultrafiltration of synthetic fruit juice [3]. Rahimi et al. [4] studied a 3D CFD simulation for predicting the water permeate flux through a microfiltration membrane. Pak et al. [5] used a numerical technique to solve the 2D flow field and convective diffusion equation for particle transport in laminar flow over a permeable surface by a tubular membrane. Li Xin et al. [6] showed the effects of promoter geometry on flow pattern.

In the present research, a cross-flow ultrafiltration process using a membrane has been studied. The flow is assumed to be laminar and incompressible. Fig.1 illustrates the simulated model of the flow in channel for validation with the experiment (3D effect is omitted). The effect of different turbulence promoter geometries has been investigated by the CFD modeling and predicted hydrodynamics parameters have been used to explain the observed results.

2. Governing Equations

The flow system was governed by the continuity equation and momentum equations. The flow in the channel and in the membrane

pores were governed by the same continuity equation, but the momentum equations were different. The membrane was treated as a porous medium, and the additional momentum loss should exist in momentum equation since membrane permeation was considered. The momentum source term was included in the momentum equation. The source term consisted of viscosity loss term and internal loss term.

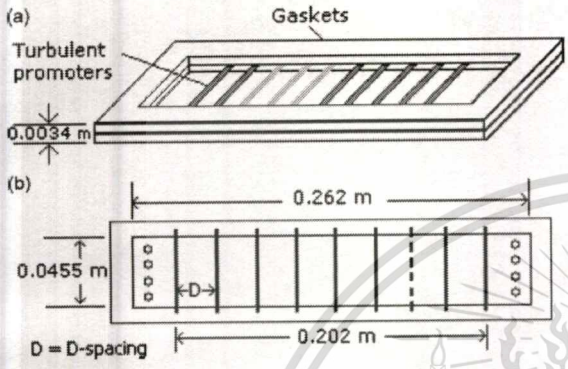

Fig.1 Model scheme (in different angles) of the flow channel used for validation [3].

Mass conservation of the flow in channel and membrane pore can be written as following.

Continuity equation:

$$\frac{\partial v_x}{\partial x}+\frac{\partial v_y}{\partial y}=0 \tag{1}$$

The momentum equations of the channel flow system in x- and y-direction were described by Eqs. (2) and (3), respectively.

x-direction

$$\rho v_x\frac{\partial v_x}{\partial x}+\rho v_x\frac{\partial v_y}{\partial y} =-\frac{\partial p}{\partial x}+\mu\left(\frac{\partial^2 v_x}{\partial x^2}+\frac{\partial^2 v_x}{\partial y^2}\right) \tag{2}$$

y-direction

$$\rho v_y\frac{\partial v_x}{\partial x}+\rho v_y\frac{\partial v_y}{\partial y} =-\frac{\partial p}{\partial y}+\mu\left(\frac{\partial^2 v_y}{\partial x^2}+\frac{\partial^2 v_y}{\partial y^2}\right)-\rho g \tag{3}$$

Also, the momentum equations of membrane pore in x- and y-direction can be expressed as:

$$\rho v_x\frac{\partial v_x}{\partial x}+\rho v_x\frac{\partial v_y}{\partial y} =-\frac{\partial p}{\partial x}+\mu\left(\frac{\partial^2 v_x}{\partial x^2}+\frac{\partial^2 v_x}{\partial y^2}\right)+S_x \tag{4}$$

$$\rho v_y\frac{\partial v_x}{\partial x}+\rho v_y\frac{\partial v_y}{\partial y} =-\frac{\partial p}{\partial y}+\mu\left(\frac{\partial^2 v_y}{\partial x^2}+\frac{\partial^2 v_y}{\partial y^2}\right)-\rho g+S_y \tag{5}$$

Porous media are modeled by the addition of a momentum source term to the standard fluid flow equations. The source term is composed of two parts: a viscous loss term (the first term on the right-hand side of Eq. (6), and an inertial loss term (the second term). To cover the case of simple homogeneous porous media, the model was given below:

$$S_i=-\left(\frac{\mu}{\alpha}v_i+C\frac{1}{2}\rho|v|v_i\right) \tag{6}$$

where S_i is the source term for the i th (x or y) momentum equation. In the porous medium domain, the viscosity coefficient and internal resistance factor in every direction should be determined. In the laminar flow, the pressure drop is direct proportional to velocity, the internal resistance might be omitted, and the porous medium model was simplified to the Darcy's principle, as shown in Eq. (7):

$$\nabla p=-\frac{\mu}{\alpha}v_i \tag{7}$$

The pressure drop in each of the two (x, y) coordinate directions within the porous region can be symbolized as:

$$\Delta p_x=\sum_{i=1}^{2}\frac{\mu}{\alpha_{xi}}v_i\Delta m_x \tag{8}$$

$$\Delta p_y=\sum_{i=1}^{2}\frac{\mu}{\alpha_{yi}}v_i\Delta m_y \tag{9}$$

The membrane was assumed to be isotropy, therefore, the transmembrane pressure was only considered in y-direction:

$$\Delta p_y = \frac{\mu}{\alpha} v_y \Delta m_y \quad (10)$$

Because pressure drop across membrane could be obtained by the equation:

$$\Delta p = \mu R_m v_y \quad (11)$$

According to (10) and (11), the $1/\alpha$ could be eventually determined.

3. Geometry and Meshing

The geometrical representation of the system is done by GAMBIT. The modeling is based on the experiment conducted by S. Pal et al. [3]. Simulations with two promoters show that the flow field keeps on repeating itself when additional promoters are added and therefore two promoters are shown in subsequent figures for clarity. However, the flux values are calculated taking into consideration the effects of all the promoters present in the flow path. The relevant values of the geometric parameters are as follows: height of the channel is 3.4×10^{-3} m, projected length of promoter is 1.68×10^{-3} m and spacing between consecutive promoters is 14.4×10^{-3} m. The grids are uniform in the region encompassing the promoter and the non-permeable upper wall of the channel. In the lower part, (from below the promoter to the membrane surface) the grid spacing decreases linearly and is smallest near the membrane surface. The final mesh geometry as shown in Fig.2 is exported to FLUENT.

4. Solution Methodology

The governing equations were solved numerically by using a commercial CFD code (FLUENT) with finite volume method (FVM). According to fundamental concept of finite volume method, the flow domain is divided into a number of cells, and the differential equations are integrated over control volume to obtain a set of algebraic equations. This process is called discretization. These equations are solved iteratively to obtain the flow field distribution of dependent variables. The standard interpolation scheme, SIMPLE algorithm and the second order upwind are activated to calculate pressure, pressure-velocity coupling and momentum, respectively.

The boundary condition for fruit juice velocity at the inlet was assumed to be uniform flow. The pressure-outlet boundary condition was used at the exit. At the wall, no-slip boundary condition was applied. About 55,000 quad cells were employed to obtain grid independent solution. The numerical results were carried out with the residuals less than 10^{-4}.

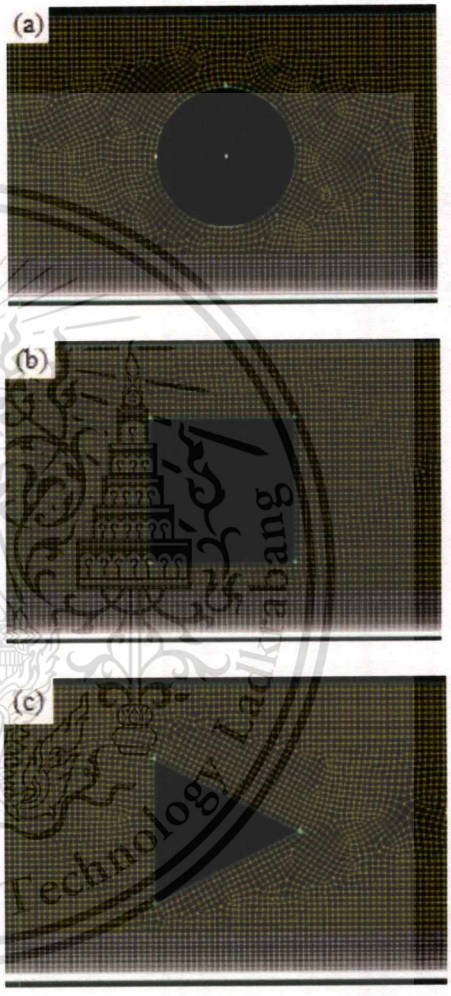

Fig.2 Mesh geometries of turbulence promoters: (a) cylinder (b) square–bar (c) prism.

5. Results and Discussions

In order to verify CFD simulations, the cross-flow ultrafiltration of fruit juice were conducted with inlet velocity of 0.16 m/s and outlet pressure of 350 kPa. The size of membrane and geometric parameters of promoters are identical as those depicted in [3]. The variation between the experimental and calculated value of permeate flux are 3.95%.

The x-velocity contours in case of using various turbulence promoter geometries are

shown in Fig. 3. The particles in the feed solution are prone to deposit on the membrane surface to form a thick cake layer, resulting in the decline of filtration flux which defines as volumetric flow rate through the membrane per its area. Fortunately, the presence of turbulence promoter not only localized turbulence around the promoters, but also interrupts development of the boundary layer on the membrane surface. Both above effects tend to reduce membrane fouling and consequently improve the performance of membrane. A conceptual view of the change in deposition thickness around a cylinder turbulence promoter, placed perpendicularly in the flow path, is presented in Fig.4. As the feed solution flows tangentially over the membrane surface, it encounters the promoters and flows around them through the gap between the promoters and the top and bottom (membrane) surfaces.

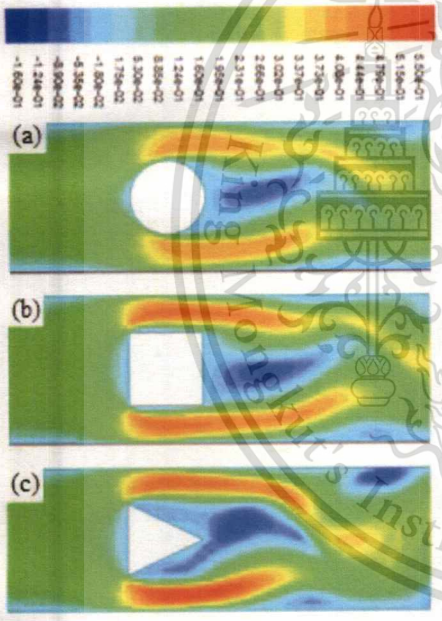

Fig.3 The x-velocity contours (m/s) around turbulence promoters: (a) cylinder (b) square–bar (c) prism.

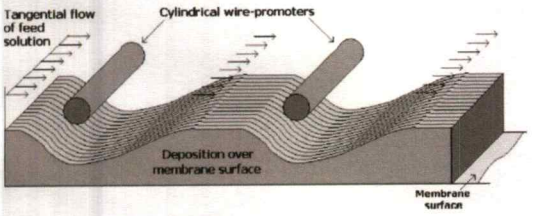

Fig.4 Conceptual view of the effect of turbulence promoters on flow and deposition [3].

The prism shape produce the highest x-velocity under the promoters as shown in Fig.3c, the permeate flux should be the highest. Therefore, all y-velocity were plotted and integrated in order to confirm the model results as shown in Fig.5 and Table 1, respectively. The velocity oscillations under turbulence promoters in the flow field are shown in Fig.5. The results show that the prism turbulence promoter can produce numerous y-velocities. Table 1 clearly shows that for all simulations with the turbulence promoter, the flux is always higher than the simulation without any turbulence promoter. This proves that the presence of turbulence promoter reduces membrane fouling thus increases the permeate flux.

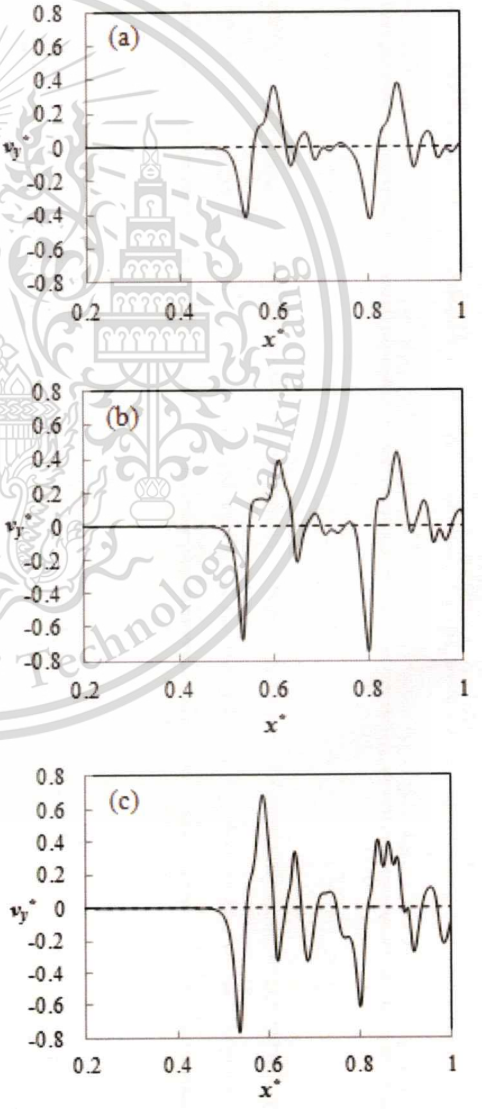

Fig.5 The y-velocity underneath turbulence promoters: (a) cylinder (b) square–bar (c) prism where $v_y^* = v_y/v_{inlet}$ and $x^* = x/L$.

Fig.6 depicts the velocity distribution pass a surface from leading edge to trailing edge of various turbulence promoters. It was found that the separation point of the cylinder turbulence promoter occurred at $x_{tp}^* = 0.7$ as for the square-bar and prism turbulence promoter occurred the same separation point but the reattachment point of the prism turbulence promoter occurred further, hence increasing eddy region and resulting in the highest permeate flux.

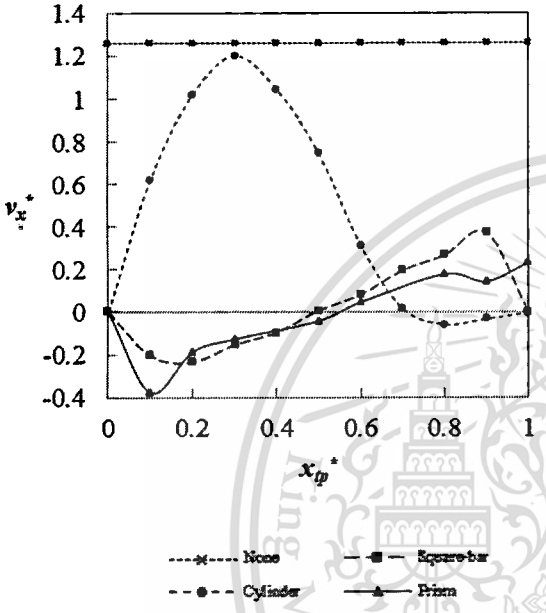

Fig.6 Velocity distributions along surface of various turbulence promoters where $v_x^* = v_x/v_{inlet}$ and $x_{tp}^* = x_{tp} / x_{total,tp}$.

The static pressure distributions in the flow path are shown in Fig. 7. For three cases, when the fluid passes each promoter, it always undergoes a sudden drop of static pressure, corresponding to the velocity fluctuation and eddy formation. From this figure, the pressure drop along the channel, the difference of static pressures between the inlet ($x^* = 0$) and outlet ($x^* = 1$), can be obtained. At an inlet velocity of 0.16 m/s and outlet pressure of 350 kPa, the pressure drop along the channel is about 0.11, 0.15 and 0.18 kPa for the cylinder, square-bar and prism promoter, respectively, which is much higher than that for no promoter (0.03 Pa). The higher pressure drop leads to the increase in additional energy cost of the membrane module. There are two main reasons accounting for the high pressure drop along the membrane channel. Firstly, the presence of turbulence promoter causes the frequent change in the flow direction and intense velocity fluctuation, which will significantly increase the frictional loss of the fluid flow. Secondly, the eddy formed behind promoters also results in the increase of energy loss.

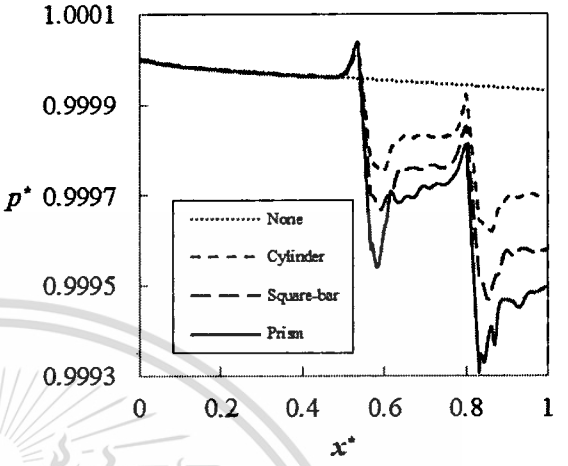

Fig.7 Static pressure distributions in the flow path where $p^* = p/p_{inlet}$.

Table 1 Performances of membrane with different types of turbulence promoters.

Promoter Geometry	Permeate Flux × 10^6 (m^3/m^2 s)	Pressure Drop (kPa)	Separation Point (-)
None	1.14	0.03	—
Cylinder	6.84 (7.11)*	0.11	0.7
Square-bar	9.5	0.15	0
Prism	11.83	0.18	0

* experimental value by S. Pal et al. [3].

6. Conclusion

The effect of different turbulence promoter geometries has been explored. The simulation results clearly show that the improved performance of cross-flow membrane ultra-filtration can be obtained by using the turbulence promoter. The insertion of turbulence promoter caused a large improvement of the permeate flux and the prism turbulence promoter can cause the largest improvement of the permeate flux with among the three types of turbulence promoters. Comparing the prism turbulence promoter with without it, the average flux can enhance up by factor of 10.

7. Nomenclature

C	inertial resistance factor (1/m)
g	acceleration of gravity (m/s^2)
L	total length of membrane in the model (m)
p	static pressure (Pa)
R_m	membrane resistance (1/m)
v_x	velocity in x-direction (m/s)
v_y	velocity in y-direction (m/s)
Re	dimensionless number of Reynolds defined by $\rho v_{inlet} w/\mu$ where w is the height of the membrane module
S_x	momentum source in x-direction (kg/m^{2}s^2)
S_y	momentum source in y-direction (kg/m^{2}s^2)
x	membrane distance (m)
x_{tp}	position on the flow path around turbulence promoter (m)
$x_{total,tp}$	projected distance from leading edge to trailing edge along turbulence promoter (m)
Δm	membrane thickness (m)
Δp	pressure drop (Pa)
μ	feed viscosity (Pa s)
ρ	feed density (kg/m^3)
α	membrane permeability (m^2)

8. References

[1] Z. Xiang-hua, Y. Shui-li, W. Bei-h, Z. Hai-feng, "Flux enhancement during ultrafiltration of produced water using turbulence promoter," Journal of Environmental Sciences, vol. 18, pp. 1077-1081, 2006.

[2] Z. Cao, D.E. Wiley, A.G. Fane, "CFD simulation of net-type turbulence promoters in narrow channel," Journal of Environmental Sciences, vol. 185, pp. 157-176, 2001.

[3] S. Pal, R. Bharihoke, S. Chakraborty, S. K. Ghatak, S. De, S. DasGupta, "An experimental and theoretical analysis of turbulence promoter assisted ultrafiltration of synthetic fruit juice," Separation and Purification Technology, vol. 62, pp. 659-667, 2008.

[4] M. Rahimi, S.S. Madaeni, K. Abbasi, "CFD modeling of permeate flux in cross-flow microfiltration membrane," Journal of Membrane Science, vol. 255, pp. 23-31, 2005.

[5] A. Pak, T. Mohammadi, S.M. Hosseinalipour, V. Allahdini, "CFD modeling of porous membranes," Desalination, vol. 222, pp. 482-488, 2008.

[6] LiXin, L. Xinping, P. Jiong, S. Yi, "Comparison of turbulence promoter geometry on flow pattern from view point of field synergy principle," Procedia Environmental Sciences, Vol. 11, pp. 1566-1573, 2011.